Journal of South American Earth Sciences 178 (2026) 106080

Contents lists available at ScienceDirect

Journal of South American Earth Sciences

journal homepage: www.elsevier.com/locate/jsames

The earliest Neogene vertebrate assemblage of the Pisco Basin, Peru

Giuseppe Marramà [a,*], Alberto Collareta [b], Giulia Bosio [b,c], Giovanni Bianucci [b], Elisa Malinverno [c], Claudio Di Celma [d], Francesco Nobile [b], Luca Pellegrino [a], Alí Altamirano-Sierra [e], Mario Urbina [e], Igor M. Villa [c], Jaime A. Villafaña [f], Alice Zanda [a], Giorgio Carnevale [a]

[a] Dipartimento di Scienze della Terra, Università degli Studi di Torino, via Valperga Caluso 35, Turin, 10125, Italy
[b] Dipartimento di Scienze della Terra, Università di Pisa, Via Santa Maria, 53, Pisa, 56126, Italy
[c] Dipartimento di Scienze dell'Ambiente e della Terra, Università degli Studi di Milano-Bicocca, Piazza dell'Ateneo Nuovo 1, Milano, 20126, Italy
[d] Scuola di Scienze e Tecnologie, Università degli Studi di Camerino, Via Gentile III da Varano 7, Camerino, 62032, Italy
[e] Departamento de Paleontologia de Vertebrados, Museo de Historia Natural-UNMSM, Jesús María, Lima, 15072, Peru
[f] Departamento de Ecología, Facultad de Ciencias, Universidad Católica de la Santísima Concepción, Concepción, 4090541, Chile

ARTICLE INFO

Keywords:
Elasmobranchii
Early Miocene
Tunga Formation
Phosphorite
Taphonomy
Paleoecology

ABSTRACT

We describe a new elasmobranch assemblage collected from phosphorite layers exposed at Cerro Tiza, in the Ica River valley (Eastern Pisco Basin, southern Peru). Chronostratigraphic and biostratigraphic data indicate an Aquitanian (Lower Miocene) age and support attribution of these strata to the Tunga Formation, thereby identifying this record as the geologically oldest Neogene vertebrate assemblage so far documented from the Pisco Basin. The assemblage comprises at least 17 species and 15 genera of selachians and batoids referable to the orders Lamniformes, Carcharhiniformes and Myliobatiformes. These taxa document a diverse marine ecosystem dominated by apex and mesopredatory species with predominantly piscivorous feeding habits, consistent with environmental conditions of elevated primary productivity. Taphonomic and paleoecological evidence indicates that the apparent dominance of a limited number of species within the Early Miocene Tunga phosphorite lag likely reflects the combined effect of both ecological structure and taphonomic filtering.

1. Introduction

The Cenozoic was characterized by major climatic changes with cyclic alternations of greenhouse and icehouse conditions (Zachos et al., 2001; Miller et al., 2005). After the cooling phase experienced at the Oligocene–Miocene transition, global temperatures rose again around 20 Ma, culminating in the middle-Miocene Climatic Optimum (MMCO; ~17–15 Ma) (Zachos et al., 2001). This interval was associated with a marked eustatic sea-level rise and the consequent expansion of shallow epicontinental seas. These conditions favoured widespread marine sedimentation, resulting in the accumulation of several fossil-rich deposits, including many that are rich with bony and cartilaginous fish remains, particularly in Europe and the Americas.

The Neogene fossil record of Pacific South America, in particular, has improved substantially over the past decades thanks to the description of new assemblages from Ecuador, Peru and Chile (e.g., Long, 1993; Suárez et al., 2006; Carrillo-Briceño et al., 2013, 2014, 2020; Villafaña and Rivadeneira, 2014, 2018; Landini et al., 2017a, 2019; Villafaña et al., 2019). However, a major knowledge gap still exists locally with respect to the chondrichthyan faunas around the Oligocene–Miocene boundary.

The East Pisco Basin (EPB) represents one of the main shelf basins that developed through the Cenozoic at the foot of the Andes (Di Celma et al., 2022). Its largely marine sedimentary fill, extending from the Middle Eocene to the Late Miocene at least, is broadly renowned for its paleontological content, which includes highly informative fossils of bony and cartilaginous fishes, marine reptiles, birds and mammals (e.g., Esperante et al., 2008; Stucchi et al., 2015; Collareta et al., 2017, 2021a, 2021b; Landini et al., 2017a, 2017b, 2019; Bianucci et al., 2018; Nobile et al., 2025; Carnevale et al., 2026), thus providing an extraordinary window into the deep-time history of the biotic communities of the Humboldt Current Ecosystem (Collareta et al., 2021b; Barron et al., 2026). To date, our knowledge of the Peruvian Miocene elasmobranch communities mainly originates from the basin fill of the EPB, specifically from the Burdigalian Chilcatay Formation and the Middle to Upper

* Corresponding author.
E-mail address: giuseppe.marrama@unito.it (G. Marramà).

https://doi.org/10.1016/j.jsames.2026.106080
Received 1 March 2026; Received in revised form 11 April 2026; Accepted 13 April 2026
Available online 16 April 2026

Miocene Pisco Formation (see the detailed historical remarks in Landini et al., 2017a, 2019). The oldest Neogene shark and ray assemblage hitherto documented from the EPB comes from the locality of Zamaca (Chilcatay Formation). This assemblage is dominated by Carcharhiniformes and Lamniformes, with *Carcharhinus brachyurus* and *Cosmopolitodus hastalis* accounting together for about 60% of the specimens (Landini et al., 2019). Conversely, the Tortonian (Upper Miocene) elasmobranch assemblage from Cerro Colorado (Pisco Formation) is dominated by a community of small mesopredator sharks (particularly *Carcharhinus brachyurus*, accounting for approximately four fifths of the specimens), suggesting the local presence of a secondary nursery and recruitment area (Landini et al., 2017a).

In this paper, we report the first occurrence of phosphorite deposits at the base of the Lower Miocene Tunga Formation exposed at the locality of Cerro Tiza. While the Tunga Formation is well-documented elsewhere in the East Pisco Basin (EPB) with its layers usually yielding scarce vertebrate evidence, the Cerro Tiza strata are unique for being home to abundant, though poorly to moderately preserved, elasmobranch (shark and ray) teeth. This study aims to (1) characterize the taxonomic composition and richness of the Cerro Tiza assemblage; (2) assess the extent to which its current faunal structure may have been shaped by taphonomic filtering, and (3) discuss the paleoecological signal recoverable from said assemblage in light of the isolated nature of the fossil material and the condensed, transgressive paleoenvironmental signature of the embedding phosphorite lag.

2. Geological and stratigraphic framework

2.1. General overview

The Peruvian forearc contains a system of NW-SE elongated Cenozoic basins subdivided into inner shelf and outer slope basins separated by trench-parallel structural highs (Thornburg and Kulm, 1981; Kulm et al., 1982; Decou et al., 2011). The East Pisco Basin (Fig. 1) is one of the inner shelf basins and is bounded by the Western Cordillera to the northeast and the Coastal Cordillera to the southwest.

The subaerial portion of the EPB, extending between the cities of Pisco and Nazca, lies immediately east of the active Nazca Ridge subduction zone (Pilger, 1981; Hampel, 2002; Contreras-Reyes et al., 2019; Ciattoni et al., 2025). Quaternary subduction of the over-thickened ridge crust resulted in flat-slab subduction (Bishop et al., 2017) and regional uplift of the overriding plate, which are interpreted to have caused cessation of volcanic activity between ~9°S and 15°S (Gutscher et al., 2000; Antonijevic et al., 2015) as well as basin inversion (e.g., Hsu, 1992; Macharé and Ortlieb, 1992; Wipf et al., 2008; Saillard et al., 2011; Ayala-Carazas et al., 2026), respectively.

The basin fill succession is up to 1000 m thick and consists of middle Eocene–Lower Pliocene sedimentary rocks recording tectonic control and sea-level changes (Dunbar et al., 1990; Di Celma et al., 2017, 2018, 2022). These rock-units were laid down intermittently, their boundaries coinciding with regional unconformities of varying magnitude that are locally accompanied by angular unconformities (DeVries, 1998; Di Celma et al., 2017). The oldest rocks exposed in the EPB, forming the Caballas, Paracas, and Otuma formations, are Eocene to early Oligocene in age and are grouped into the Megasequence P, whereas the overlying Miocene Tunga, Chilcatay, and Pisco formations constitute the Megasequence N (Dunbar et al., 1990; DeVries, 1998, 2017; DeVries et al., 2017, 2024; DeVries and Jud, 2017; Di Celma et al., 2022).

The present paper deals with the marine strata of the Tunga Formation, the oldest recognized rock-unit of Megasequence N. This stratigraphic sequence, originally described by DeVries et al. (2024), is poorly preserved and occurs as laterally discontinuous, unconformity-sandwiched sediment wedges. Diatom biostratigraphic data indicate that in its type section (base at 14°11′24″S - 76°07′09.06″W, top at 14°11′14.52″S - 76°07′1.68″W) the Tunga Formation was deposited between roughly 21.6 and 20.5 Ma (DeVries et al., 2024). This age is supported by U–Pb zircon dating of a basal ash bed, which yielded a weighted mean age of 20.58 ± 0.13 Ma, confirming an earliest Miocene (Aquitanian) age. Accordingly, the stratigraphic unit correlates well with a sedimentary package reported by Bosio et al. (2022) at Quebrada Perdida (21.8–20.1 Ma), near Media Luna (Fig. 1B), which those authors attributed to the Chilcatay Formation before the Tunga formation was defined.

2.2. The Tunga Formation at Cerro Tiza

This study reports for the first time strata of the Tunga Formation exposed in the Ica River Valley. Along the southern side of Cerro Tiza (Fig. 1B and 2), the Tunga Formation forms a strongly wedge-shaped sediment package, reaching up to approximately 30 m in thickness at its maximum (Fig. 1C). It unconformably overlies the earliest Oligocene portion of the Otuma Formation (Gastaldello et al., in press) and is, in turn, overlain by strata of the succeeding Chilcatay Formation (Fig. 2A). At this site, its basal unconformity (TE0) is veneered with a 40-cm-thick, poorly sorted, coarse-grained pavement (Fig. 2B), including a mixture of closely-packed, granule- and pebble-sized phosphatic nodules, reworked cobble-sized clasts of dolomite-cemented siltstones from the underlying Otuma Formation showing different bioerosional traces (Fig. 2C), internal molds of gastropods and articulated bivalves, shark teeth (Fig. 2D), and skeletal elements of marine mammals set in a poorly cemented sandy matrix. When considered collectively, the stratigraphic position, grain size, clast composition, lateral extent, and degree of bioerosion of the clasts indicate that the basal unconformity and the overlying coarse-grained pavement represent a wave-ravinement surface and an associated condensed lag deposit, respectively, formed in the shoreface through erosion and low net sediment accumulation at the onset of transgression. (Bosio et al., 2024). In particular, as phosphate nodules only form below the sediment-water interface, their abundance indicates condensation in the context of coastal onlap under a regime of repeated alternation of episodes of sediment accumulation and wave reworking and winnowing (dynamic bypass *sensu* Kidwell, 1989). The phosphate-rich deposits are directly overlain by about 5 m of intensely bioturbated, grey-green shallow marine fine-grained sandstones. Overlying the sandstones is a discrete volcanic ash layer that, in turn, passes upwards into a package of poorly exposed offshore diatomaceous siltstones.

To constrain the age of the Tunga Formation within the study area, an integrated biostratigraphic and tephrochronologic approach is provided herein.

3. Material and methods

3.1. Chronostratigraphy

In the field, a tephra layer (CTZ-T129) exposed a few meters above the fossil teeth-rich phosphorite bed was sampled, avoiding weathered material and extraneous particles. Two samples were collected: one from the base of the layer (B), where large phenocrysts are concentrated, and one from the top (A), where fine-grained phenocrysts and finer glass shards dominate. Ash from sample CTZ-T129B was processed for grain-size and geochemical characterization and subsequent dating following the protocol outlined in Bosio et al. (2019, 2020). Grain-size characteristics of the selected layer were determined using a Malvern Mastersizer 2000E™ laser granulometer at the Università di Milano-Bicocca, and the resulting data were processed with the GRADISTAT software (Blott and Pye, 2001). After grain-size analysis, the ash was wet-sieved into 500, 250, 125, and 63 μm size fractions. The 250–500 μm fraction was mounted in resin, polished, and then analyzed for major-element composition using a JEOL 8200 Superprobe at the Università degli Studi di Milano, operating at 15 kV accelerating voltage and 5 nA beam current. Beam diameters of 3 μm and 10 μm were adopted for biotite phenocrysts and volcanic glass shards, respectively. Two hand-picked

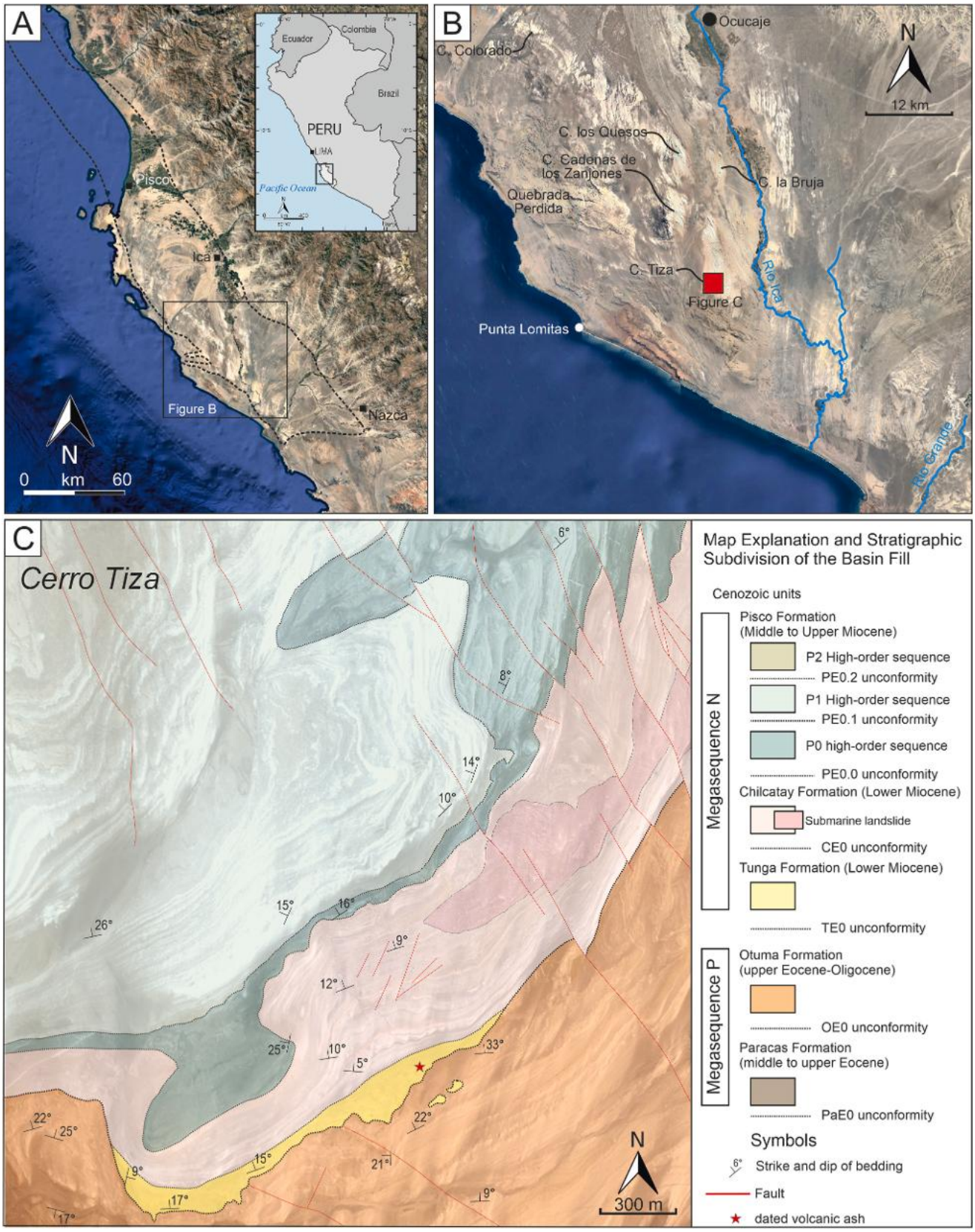

Fig. 1. Geological and stratigraphic setting of the study site. A, aerial view of the East Pisco Basin (from Google Earth satellite imagery); inset: location of the East Pisco Basin in south-central Peru; B, magnification of the area shown in A with the position of some relevant fossil localities; C, detailed geological map of the Cerro Tiza locality (redrawn and modified from Di Celma et al., 2022).

Fig. 2. The study area at Cerro Tiza (East Pisco Basin, Peru). A, landscape view of the lower Tunga strata. B, outcrop view of the basal lag deposit of the Tunga Formation. C, close-up of a large, heavily bioeroded cobble-sized clast of dolomite-cemented siltstone within the basal lag deposit. D, close-up of an *Otodus chubutensis* tooth (MUSM 5297) within the basal lag deposit.

mg-sized biotite separates were irradiated together, a 1.8 mg dry grain aliquot and an 11 mg aliquot, at the McMaster University nuclear reactor for ^{39}Ar–^{40}Ar dating. In order to control the vertical flux gradient, several disk wraps of Fish Canyon sanidine (FCs age: 28.172 ± 0.028 Ma following Rivera et al., 2011) and MMhB horneblende (MMhB age: 523.2 ± 0.9 Ma following Spell and McDougall, 2003) were interlayered with the sample disk wraps. The irradiation intensity factor J was interpolated for each sample from the parabolic equation defined by the J values of the FCs monitors. Noble gas isotopic compositions were determined through a step-heating method using a Nu Instruments Noblesse mass spectrometer at the Università degli Studi di Milano-Bicocca, with data corrections and age calculations performed according to the protocols described in Bosio et al. (2020). The isochron calculations, weighted averages, and estimates of excess scatter (via MSWD and probability parameters) were calculated using Isoplot (Ludwig, 2012).

3.2. Biostratigraphy

Five samples (CTZ-130, CTZ24-D36 to D39) from the Tunga Formation in the Cerro Tiza area were prepared for biostratigraphic analyses as standard smear-slides (Bown and Young, 1998) using rectangular cover slips (24 × 40 mm). Two to three whole slides were examined for each sample using an Olympus BX50 light microscope with immersion oil at 1000 × with parallel nicols to detect diatom and silicoflagellate marker taxa.

3.3. Macrofossil material

The macrofossil content consists of 751 isolated fossil teeth that have been collected by the authors between 2021 and 2024 from the phosphorite tooth-bearing levels of the Tunga Formation exposed at Cerro Tiza. Of these, 533 are moderately to well preserved, allowing for taxonomic identification. The remaining 218 are only represented by crown fragments, but the absence of recognizable diagnostic traits precludes identification at low taxonomic level. Consequently, these latter were excluded from the analyses, although they provide relevant information for assessing the taphonomic implications that are discussed below.

The sampling method consisted of random surface prospecting. The fossil specimens were then directly investigated with hand lenses, microscopes and macrophotography. Optical photographs were obtained using a Canon EOS R10 camera coupled with a macro lens Canon RF 100 mm F/2.8. Teeth were measured to the nearest 0.01 mm by using dial callipers and determined following Cappetta (2012), Landini et al. (2017a, 2019), Villafaña et al. (2020, 2024), Höltke et al. (2022), Chávez-Hoffmeister and Villafaña (2023) and Maisch et al. (2025), among others. Morphological tooth terminology mostly follows Cappetta (2012). All specimens are housed in the paleontological collections of the Museo de Historia Natural de la Universidad Nacional Mayor de San Marcos, Lima, Peru (MUSM).

3.4. Diversity and ecological inference methods

In the present study, the term “diversity” refers to species richness, that is, the number of species recorded in the assemblage. For analyses concerning diversity and ecological relationships, taxa identifiable only to the genus level (e.g., *Rhinoptera* sp.) were treated as representing a single species, whereas taxa identified in open nomenclature (e.g., *Mitsukurina* cf. *lineata*) were treated as representing the closest confidently identified species.

Dietary preferences were inferred through an integrated approach combining the assessment of dental morphology (following Cappetta, 2012) and ecological comparisons with the closest extant taxon at

species level (when fossils belong to extant genera) or at family level (when fossils belong to extinct genera), implementing information with literature. Although living elasmobranch have wide ranges of prey items, each family has specific food preferences (e.g., Cortés, 1999) that could be used to infer the dietary preferences of their fossil relatives (see Carrillo-Briceñõ et al., 2019; Marramà et al., 2021). Information on the trophic ecology of modern taxa used to infer the diets of fossil taxa was chiefly derived from Nelson et al. (2016) and FishBase (Froese and Pauly, 2025). Likewise, reconstructions of habitat and bathymetric affinities for fossil taxa were based on the environmental preferences of their extant counterparts, following Froese and Pauly (2025). Because the Cerro Tiza assemblage is entirely based on isolated teeth, and considering that it includes several taxa identified at genus-level only or even in open nomenclature, the ecological assignments proposed here should be regarded as broad working hypotheses rather than high-resolution assessments. In particular, dietary, habitat and bathymetric inferences are intended to identify general ecological tendencies within the assemblage, not to provide precise estimates for the Cerro Tiza paleobiotope.

Furthermore, we compared the taxonomic composition of the Early Miocene elasmobranch fauna from Cerro Tiza with those known from other seven roughly coeval (Lower to Upper Miocene) deposits of the East Pacific coast of South America, following in part the comparative procedure applied by Marramà et al. (2021). Specifically, hte elasmobranch assemblages considered in our analysis include: the Lower Miocene fossil-bearing strata of the Chilcatay Formation at Zamaca, Peru (17 genera; Landini et al., 2019); the Upper Miocene strata of the Pisco Formation at Cerro Colorado, Peru (15 genera; Landini et al., 2017a); the Oligocene-Miocene deposits of the Dos Bocas Formation at Montañita-Olón site, Ecuador (22 genera; Carrillo-Briceño et al., 2020); the Lower Miocene strata of the Navidad, Ranquil and Lacui Formations of Chile (12 genera; Villafaña et al., 2019); the Middle Miocene to Lower Pliocene outcrops of the Bahia Inglesa Formation at Los Dedos, Chile (32 genera; Chávez-Hoffmeister and Villafaña, 2023); and the Upper Miocene horizons of the Bahia Inglesa Formation at Econssa, Chile (12 genera; Villafaña et al., 2025).

Since these assemblages have very different sample abundances (ranging from 62 to 3918 specimens), we relied on Shareholder Quorum Subsampling (SQS) to standardize taxonomic richness because classical rarefaction equalizes samples by individual count rather than by sampling completeness, a limitation known to artificially compress richness differences among assemblages (Gotelli and Colwell, 2001; Alroy, 2010). In turn, SQS standardizes samples by coverage, the fraction of the community represented by the observed taxa, providing fairer comparisons among datasets with different abundance distributions (Alroy, 2010; Chao and Jost, 2012). Unlike classical rarefaction, which standardizes samples to a fixed number of individuals, SQS uses coverage as the basis for comparison. Coverage (Good's u values) represents the proportion of the community's individuals that belong to taxa detected in the sample. A coverage value of 1 means that all taxa in the population are represented, whereas a coverage of 0.5 or less indicates that the sampled taxa collectively account for no more than half of the individuals in the actual community.

The taxonomic diversity of the seven elasmobranch assemblages has been then crosschecked with different diversity indices that are insensitive to sample size and describe different patterns of diversity such as the alpha richness and evenness (Magurran, 2004; Marramà et al., 2016), including the Dominance, Berger-Parker, Simpson and Shannon indices.

To evaluate the taxonomic similarity among these assemblages, we used the Dice correlation index (also known as Sørensen coefficient), which quantifies resemblance among two or more communities based on presence-absence data (Dice, 1945; Sørensen, 1948). This metric is widely applied in studies of modern and fossil ecosystems, and is generally considered one of the most reliable presence/absence-based similarity measures (Southwood and Henderson, 2000; Magurran, 2004; Villafaña et al., 2020). All analyses were performed at the genus level in order to reduce errors from incomplete fossil data (e.g., missing or indeterminate species), acknowledging the fossil record's biases (see Benton et al., 2011). Although the Dice index can be influenced by incomplete taxonomic lists (Jost et al., 2011), we consider the taxonomic record of all the assemblages as effectively comprehensive as shown by results from the Shareholder Quorum Subsampling. Taxonomic similarities were further explored using a cluster analysis to identify hierarchically structured associations reflecting shared paleoecological and paleoenvironmental affinities.

All analyses were performed using the software package PAST v. 5.3 (Hammer et al., 2001)

4. Results

4.1. Chronostratigraphy

The CTZ-T129B sample, collected in the lower portion of the ash layer, is characterized by a unimodal and poorly sorted grain-size distribution (Fig. 3A), falling within the sediment class of very coarse silty medium sand (Blott and Pye, 2001). The deposit consists of 86.4% sand and 13.6% mud, with the preferential accumulation of larger phenocrysts at the base of the ash layer, consistent with primary deposition from distal fallout (Griggs et al., 2014). Petrographic analysis of the 250–500 μm size fraction (Fig. 3B) reveals abundant, low vesiculated glass shards with a bubble-wall morphology associated with sufficiently fresh biotite phenocrysts, and subordinate feldspar and quartz phenocrysts, confirming the primary airfall origin (Lowe, 2011; Griggs et al., 2014). Electron microprobe analyses of glass shards and biotite indicate a chemically homogeneous population, with rhyolitic glass compositions and biotite Mg/(Mg + Fe + Mn) ratios clustering within a narrow range. Alkali contents are systematically lower than the stoichiometric value of 2 atoms per formula unit (apfu), ranging from 1.65 to 1.76 apfu (Fig. 3C). Accordingly, the irradiation-derived K content is 7.07%, below the stoichiometric value of 8%, suggesting moderate alteration in the marine environment (Villa and Bosio, 2023). In addition, about one-fifth of the microprobe analyses on biotite grains have high Al concentrations, compatible with sub-μm feldspar intergrowths, as also supported by the Cl concentrations less than half of the other spot analyses on biotite. Note that microprobe analyses demonstrate that the Ca/K ratio of biotite proper is < 0.002 in CTZ-T129B. Since the Ca/K ratio from the Ar analysis is at least 15 times higher, it follows that in all steps one or more Ca-rich phases were being degassed in addition to biotite. This weakens the identification of the inferred “pure primary biotite” signature.

Consequently, it is necessary to rely on two features of the ^{39}Ar–^{40}Ar systematics that are sometimes neglected in favor of the more palatable, but less informative, age spectrum diagram. The first are three-isotope correlation diagrams (Turner, 1988), the second are differential Ar release diagrams (Zimmermann, 1970); their combined use was recently reviewed by Montemagni and Villa (2025). Isotope correlation diagrams provide the compositional signature of the minerals degassed in a polymineralic sample (note carefully that even prolonged handpicking of a mineral separate can never eliminate the ubiquitous sub-μm retrograde reaction products). The compositional indicators that are relevant for biotite sample CTZ-T129B are the Ca/K ratio, which should be near zero in stoichiometric micas, and the Cl/K ratio, which should be constant, as Cl-uniformly substitutes for OH- in the mica structure. In context with the compositional signature, it is clearly established that different phases (such as alteration clays, micas, and feldspars) all degas Ar at different characteristic furnace temperatures. The peak temperature of the differential Ar release of biotite sensu stricto is between 800 and 1000 °C, that of feldspars above 1100 °C, and that of secondary clays (talc, serpentine) below ca. 700 °C.

In the present case, the variation of the compositional signature forbids the use of isochrons, because the heterochemical phases present

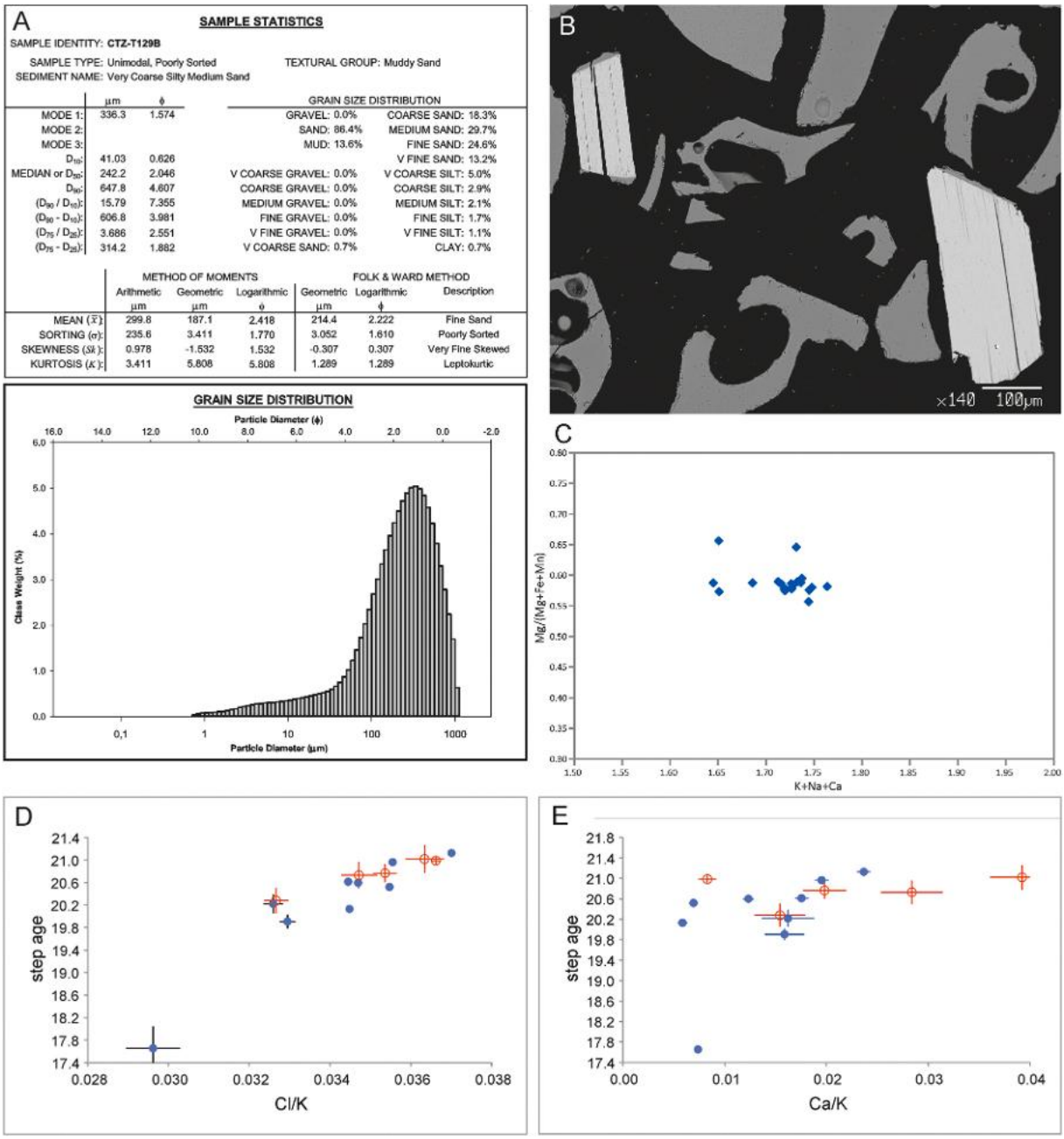

Fig. 3. Characterization of the dated volcanic ash sample CTZ-T129B. A) Grain-size data and grain-size distribution curve, obtained with the Grain Size Analysis Program GRADISTAT (Blott and Pye, 2001). In the diagram, particle diameter is shown as both micrometers (µm) and phi (φ). B) BSE image of the 250- to 500-µm-size fraction showing low vesiculated glass shards with a bubble-wall morphology (dark grey) and biotite phenocrysts (light grey). Note the glass rim surrounding the biotite phenocrysts. C) Biotite Mg/(Mg + Fe + Mn) v. K + Na + Ca diagram showing the biotite composition of the analyzed tephra. To obtain statistically significant results, the EPMA analyses were performed on 10 biotite crystals (both rim and core for each crystal). D) Step age vs Cl/K diagram showing the heating steps of both small and large aliquot of biotite phenocrysts. E) Step age vs Ca/K diagram showing the heating steps of both small and large aliquot of biotite phenocrysts. Data are shown as open and filled circles, respectively, with 1σ error bars. In most steps of the large aliquot, the uncertainty is smaller than the symbols.

in the separate are not cogenetic. Indeed, regressions through the data points are overdispersed, or have "extraterrestrial" ordinate intercepts, or both; this proves that the regressions are not legitimate. Some insight is provided by the correlation graph of Age vs Cl/K (Fig. 3D), which shows that younger step ages correspond to analytically well resolved low Cl/K ratios. The spread in the Cl/K ratios is 25%, that in ages is 20%. This is interpreted as a predominantly binary alteration trend, with the formation of a young, Cl-poor secondary phase. Judging from the very high furnace temperatures corresponding to the young endmember of this trend, the secondary phase could be hypothesized as feldspar. A similar trend, with an essential difference, is shown by the Age vs Ca/K diagram (Fig. 3E). The difference is that the spread in the Ca/K ratios is 473%; this requires the presence of one or more secondary K-poor or K-free phases in addition to the K + Cl bearing phases of Fig. 3D and makes a straightforward interpretation less constrained. By focusing the attention on the steps at the upper right end of the trend in Fig. 3D, we note that three of the four steps nearest to the supposedly primary Cl/K signature are degassed below 1000 °C; the variation interval of the four step ages is between 20.96 and 21.13 Ma. The degassing temperatures are compatible with the Ar release from mica. If this identification is correct, we can select the step with the most extreme isotopic signature (step 3 of the large aliquot, Cl/K = 0.03701 ± 0.00014, t = 21.13 ± 0.10,

both at 95% confidence level) as the least altered signature (Table S1). For this reason, the final age estimates for CTZ-T129 tephra is 21.13 ± 0.10 Ma. Note that this age estimate is not comparable to similar-looking age estimates from the literature, as no quantitative assessment of possible diagenetic alteration was reported for any of them. All the analytical data are reported in Table S1 (see Supplementary Material).

4.2. Biostratigraphy

Samples from the Tunga Formation are dominated by lithogenic material with a minor contribution of siliceous microfossils and lack calcareous microfossils. Diatoms and silicoflagellates are scarce, and exhibit a low biodiversity assemblage, with moderate to bad preservation and only a few intact skeletons. Among diatoms, the following marker species were identified: *Azpeitia oligocenica* (34.5–20.6 Ma; Coenen et al., 2025), *Cavitatus jouseanus* (28.5–6.8 Ma, Coenen et al., 2025), *Cavitatus linearis* (late Oligocene to ca. 15 Ma; Akiba et al., 1993), *Coscinodiscus rhombicus* (28.6–17.3 Ma; Lazarus et al., 2014), *Raphidodiscus marylandicus* (23.5–16.5 Ma, Coenen et al., 2025). Among silicoflagellates, the marker species *Corbisema flexuosa*, *C. triacantha*, *Dictyocha brevispina*, *Naviculopsis biapiculata* and *N. lata* represent a typical assemblage of the early Early Miocene *Naviculopsis lata* zone (Bukry, 1981, McCartney et al., 2020). Collectively, the siliceous assemblage allows to constrain the succession between 23.5 Ma (FO of *R. marylandicus*) and 20.6 Ma (LO of *A. oligocenica*), an age range that is consistent with the 21.8–20.6 Ma time frame assigned by DeVries et al. (2024) to the Tunga Formation.

4.3. Systematic paleontology

Class Chondrichthyes Huxley, 1880
Subclass Elasmobranchii Bonaparte, 1838
Superorder Galeomorphii Compagno, 1973
Order Lamniformes Berg, 1937
Family Mitsukurinidae Jordan, 1898
Genus *Mitsukurina* Jordan, 1898
Mitsukurina cf. *lineata* (Probst, 1879)
(Fig. 4A)

Material. Two fragmentary teeth, including MUSM 5291 (Fig. 4A).

Description. These two tooth fragments, the tallest reaching 26 mm in height, originate from the lingual face of slender, high, narrow crowns of the lower anterior teeth. The lingual surface is strongly convex transversely and S-shaped in profile view, and bears well-defined, apicobasal plications that arise at the crown base and fade gradually around mid-height of the crown. The individual folds are straight to slightly sinuous, closely spaced near the base, and diminish in relief apically. No transverse ornaments, nodes, or striae are present between the folds, and the cutting edges are smooth, approaching the crown base without serrations.

Remarks. The observed traits match with the descriptions and figures of the lingual face of anterior teeth of *Mitsukurina lineata*, *M*. cf. *lineata* or

Fig. 4. Lamniformes from the Early Miocene phosphorites of the Tunga Formation at Cerro Tiza (Ica Desert, Peru). A, *Mitsukurina* cf. *lineata* (Probst, 1879) (MUSM 5291), lower anterior tooth; B, *Alopias superciliosus* Lowe, 2011 (MUSM 5292), upper lateral tooth; C, *Alopias vulpinus* (Bonnaterre, 1788) (MUSM 5293), upper lateral tooth; D, *Anotodus retroflexus* (Agassiz, 1834) (MUSM 5294), antero-lateral tooth; E, *Pseudocarcharias* sp. (Matsubara, 1936) (MUSM 5295), lower anterior tooth; F, *Carcharias taurus* Rafinesque, 1810 (MUSM 5296), lower anterior tooth. In image A, tooth is figured in lingual (1) and profile (2) views; in images B to F, teeth are figured in lingual (1), labial (2), and profile (3) views. Scale bar = 10 mm.

Mitsukurina sp. from the Lower Miocene of the Molasse Basin, Costa Rica and Ecuador (Carrillo-Briceño et al., 2020; Villafaña et al., 2020; Laurito et al., 2014). The preserved relief, spacing and apical attenuation of the folds are consistent with lower anterior positions of *Mitsukurina*, rather than with teeth of carchariids and odontaspidids (which exhibit a different fold architecture) or lamnids (which typically lack basal lingual plications) (Cappetta, 2012). These observations support our referral to *Mitsukurina*, while the fragmentary preservation prevents a definitive species-level identification. These specimens represent the first occurrence of *Mitsukurina* in the Miocene of Peru and the southernmost record of the genus in the eastern Pacific, therefore reinforcing the tropical to warm-temperate distribution of the genus across the East Pacific since at least the Early Miocene (e.g., Laurito et al., 2014).

Family Alopiidae Bonaparte, 1835

Genus *Alopias* Rafinesque, 1810

Alopias superciliosus Lowe, 1841

(Fig. 4B)

Material. Four upper teeth, including MUSM 5292 (Fig. 4B).

Description. The largest specimen attributed to *Alopias superciliosus* is a moderately large upper lateral tooth, reaching up to 23 mm in total height (Fig. 4B). The teeth exhibit the diagnostic features of lamniform sharks of the family Alopiidae, which are characterized by a slender, elongated, smooth-edged cusp devoid of lateral cusplets. The crown is triangular and labiolingually compressed, with a tall and slightly distally inclined cusp. The cusp is narrow and acutely pointed, with smooth, continuous cutting edges that extend down to the base of the crown. The labial face of the crown is flat to weakly convex, overhanging the root along a gently arched crown-root junction (Fig. 4B2). The lingual face is convex and bulging, particularly in its basal third, where it merges with the lingual protuberance of the root. In profile view, the crown appears as slightly sigmoidal, gently curving lingually toward the apex. There are no lateral cusplets. The incomplete root has a low and robust appearance, with well-separated lobes, slightly expanded laterally to form a moderately large basal outline. The lingual protuberance is well developed, rounded, and bears a pronounced nutritive groove containing a large central foramen (only visible in one specimen).

Remarks. The overall crown-root morphology corresponds to the generalized *Alopias* pattern. Specifically, it closely resembles that of the extant bigeye thresher, *A. superciliosus*, by exhibiting a narrow crown with a less pronounced lingual inclination than typical of *A. vulpinus*, providing the tooth with a more upright appearance and open root lobes. The fossil record of *A. supercilious* dates back to the Oligocene and has worldwide distribution (Höltke et al., 2024). Miocene occurrences from South America have been reported from Chile, Peru, Colombia and Venezuela (Carrillo-Briceño et al., 2016a, 2016b; Landini et al., 2019; Villafaña et al., 2019).

Alopias vulpinus (Bonnaterre, 1788)

(Fig. 4C)

Material. A single, partially preserved upper lateral tooth, MUSM 5293 (Fig. 4C).

Description. The only specimen attributed to *Alopias vulpinus* is a small upper lateral tooth measuring 9 mm in total height. The crown is low and distinctly broad, with a rather flat labial face. It is slightly inclined distally and exhibits a subtle lingual curvature in profile view. Both the labial and lingual faces are smooth and entirely devoid of ornamentation or striae. The labial face is flat to gently convex and overhangs the root with a distinct shoulder, while the lingual face is more convex, displaying a weak median bulge near the base. The cutting edges are smooth, continuous and sharp, extending from the apex to the base of the crown. The enameloid is smooth and featureless under magnification. Lateral cusplets and heels are absent. The root is low, massive and bilobate, with broad, well separated lobes, and a weak but distinct lingual bulge. The basal margin of the root is slightly arched.

Remarks. Compared to *A. superciliosus*, the cusp of the common thresher, *A. vulpinus*, is broader and stouter, and the root lobes are shorter and more massive, resulting in a more compact overall appearance (Cappetta, 2012). Its fossil record likely dates back to the late Oligocene, with a paleogeographic distribution that basically reflects the modern one (Höltke et al., 2024; Villafaña et al., 2024). The Miocene records of *A. vulpinus* indicate a wide range across tropical, subtropical and temperate waters of all the Americas and Europe (Villafaña et al., 2024), often besides its extant congener, *A. supercilious* (Landini et al., 2019; Villafaña et al., 2019).

Genus *Anotodus* Le Hon, 1871

Anotodus retroflexus (Agassiz, 1834)

(Fig. 4D)

Material. A single upper anterior tooth and ten moderately preserved lower anterolateral teeth, including MUSM 5294 (Fig. 4D).

Description. The crown of the single upper anterior tooth is triangular, erect and almost symmetrical, with a rather large base, which is slightly constricted. The cusp is slightly inclined lingually, and has a convex lingual face and a rather flat or slightly concave labial face. The cutting edges are salient and completely smooth. The basal limit of the crown is concave in labial view and forms a distinct bulge overhanging the root. The root is lacking in most samples.

The lower anterolateral teeth of *Anotodus retroflexus* are medium-sized, up to 23 mm in total crown height. They are characterized by a high, slender, recurved cusp that defines the species' diagnostic "retroflexed" profile. The crown consists of a single, elongated cusp that is distally inclined and features a broad base; it often exhibits a sigmoid curvature in labiolingual profile. The cutting edges are smooth and continuous, and extend from the apex to the base of the crown without serrations. The labial crown face is flat to weakly convex, whereas the lingual face is flat to slightly convex.

No lateral cusplets or accessory heels are present in both upper and lower teeth and the enameloid surface is completely smooth, with no ornamentation or striations.

Remarks. This species was originally described by Agassiz (1834) as *Oxyrhina retroflexa* based on teeth from the Miocene Europe. Subsequent authors transferred the species to *Isurus*, treating *Anotodus agassizii* Le Hon, 1871 as a junior synonym of *Isurus retroflexus*. Later, Herman (1979) resurrected the genus *Anotodus*, with *A. retroflexus* as a member of the thresher shark family Alopiidae. Since the retrieval of the genus *Anotodus* by Cappetta (2012), this combination has been followed by several studies on Neogene elasmobranchs (Carrillo-Briceñ et al., 2019; Szabó et al., 2021). In view of the most recent systematic literature and the alopiid affinities argued by Herman (1979) and Cappetta (2012), we regard *Isurus retroflexus* as an obsolete combination and prefer using *Anotodus retroflexus* (Agassiz, 1834).

Family Pseudocarchariidae Compagno, 1973

Genus *Pseudocarcharias* Cadenat, 1963

Pseudocarcharias sp.

(Fig. 4E)

Material. Nine lower anterior teeth, including MUSM 5925 (Fig. 4E)

Description. The lower anterior teeth are small to medium-sized, their crowns reaching up to 25 mm in total height, and characterized by a gracile, *Carcharias*-like morphology. The crown is high, narrow, slender and erect, and tapers into a sharp apex. The cutting edges are smooth; they are well marked but occupy only the apical third of the crown, with the mesial one being shorter, whereas the base of the crown lacks cutting edges and is nearly circular in cross-section. In labial view, the crown is almost symmetrical, whereas the cusp is only weakly inclined distally. The labial face is flat to slightly convex, overhanging the root in its basal third, and features a faint concavity close to its base. The lingual face is more distinctly convex. In profile view, the crown strongly bends lingually, being slightly sigmoid in some teeth, whereby the tooth apex faintly curves labially.

Remarks. The genus *Pseudocarcharias* is characterized by a combination of features that distinguish it from all other lamniforms: a slender, smooth-edged cusp without cusplets; a low, bilobate root with a prominent lingual protuberance; and a relatively narrow root-crown junction. These traits place *Pseudocarcharias* outside the Carchariidae,

Lamnidae and Odontaspididae, supporting its recognition as the sole member of a distinct, monotypic family (Compagno, 1973; Cappetta, 2012).

Pseudocarcharias kamoharai (Matsubara, 1936) is the sole extant representative of the family Pseudocarchariidae, a lineage that first appears in the fossil record in the Lower Miocene and has since persisted with remarkably little morphological change, although large-sized teeth exceeding 20 mm (teeth of the extant species are below 15 mm) might suggest intraspecific variation or be the result of "gigantism" (e.g., Reichmann et al., 2025). For this reason, we prefer to maintain an open nomenclature for our specimens. Fossil occurrences referred to *Pseudocarcharias* have been reported from the Early Miocene to Pliocene of several localities of the Americas and Europe (e.g., Carrillo-Briceño et al., 2015; Landini et al., 2017a; Höltke et al., 2022), indicating a cosmopolitan distribution in tropical and subtropical seas during the Neogene.

The continuity of this morphology from the Miocene fossils to the living *P. kamoharai* supports the interpretation of *Pseudocarcharias* as a highly conservative lineage, retaining ancestral lamniform characters while occupying a specialized ecological niche as a small pelagic mesopredator. As such, fossils referred to *Pseudocarcharias* likely represent members of the same evolutionary lineage as the extant species rather than an extinct congener.

Family Carchariidae Müller and Henle, 1838
Genus *Carcharias* Rafinesque, 1810
Carcharias taurus Rafinesque, 1810
(Fig. 4F)

Material. 13 lower anterior and anterolateral teeth, including MUSM 5296 (Fig. 4F).

Description. The teeth are medium-sized, with the largest crown in our sample being 24 mm tall (Fig. 4F). The crowns of lower anterior teeth are triangular in labial view and exhibit a sigmoid profile. The labial surface is rather flat, whereas the lingual surface is strongly convex and mostly smooth. The cutting edges are smooth and terminate before reaching the crown base. Small, low, triangular lateral cusplets flank the main cusp. In the lower anterolateral teeth, the cusp becomes asymmetrical, broader and more labiolingually flattened. In the upper lateral teeth, the crown curves distally. The mesial cutting edges are concave near the base and convex toward the tip, whereas the distal edge is concave close to its base and then straightens.

Remarks. The very high, sharp, sigmoid main cusps of these anterior teeth closely match those of *C. taurus* (see Cappetta, 2012). Although this taxon is often diagnosed by the presence of lingual folds ascending high on the crown, their absence is also compatible with this living taxon (e.g., Cigala-Fulgosi et al., 2009; Reinecke et al., 2011; Cappetta, 2012). In the fossil record of the Pacific coast of South America, materials referable to *Carcharias taurus* or *C.* cf. *taurus* have been widely recorded from Lower Miocene to Pliocene localities (Landini et al., 2017a, 2019).

Family Otodontidae Glikman, 1964
Genus *Otodus* Agassiz, 1834
Otodus chubutensis (Ameghino, 1901)
(Fig. 5A)

Material. 18 partially preserved to fragmentary teeth, including MUSM 5297 (Fig. 5A).

Description. The largest and best-preserved specimen referable to *Otodus chubutensis* is a lower lateral tooth that reaches up to approximately 80 mm in total height.

This tooth is large and triangular, taller than wide, with an unicuspid crown that is distally inclined and labiolingually compressed. The cutting edges are finely serrated from the crown apex to the base. In labial or lingual view, both cutting edges are slightly sigmoid, being convex toward the apex and base, and slightly concave at mid-length. The crown preserves a distinct but reduced distal lateral cusplet that is separated from the main cusp by a small notch. The labial face of the crown is nearly flat, whereas the lingual face is convex and overhangs the root above a partially preserved neck on the lingual base. The root is only partially preserved but exhibits a robust and bilobate structure, with widely separated lobes that likely formed a wide, obtuse angle.

Remarks. Teeth of *O. chubutensis* typically differ from those of its close congener, *O. megalodon*, in retaining distinct lateral cusplets (Perez et al., 2019). However, because ontogenetic variation within the *Otodus* lineage may affect the development and persistence of cusplets, this character alone should be used with caution. Our species-level referral is therefore based on the overall tooth morphology and size as well as on the Aquitanian age of the deposit which the studied material originates from. In contrast, large lamnids such as *Cosmopolitodus hastalis* or *Isurus oxyrinchus* lack serrations and cusplets, whereas *Parotodus* has bulky, non-serrated crowns with a different root architecture, making misidentification unlikely when serrations and cusplets co-occur (Cappetta, 2012). Chronostratigraphically, *O. chubutensis* is characteristic of the Lower Miocene, being commonly recorded in Aquitanian and Burdigalian assemblages worldwide (e.g., Ameghino, 1901; Aguilera et al., 2017; Domingo Carrillo-Bricenõ et al., 2019; Landini et al., 2019), and even used as an age indicator, whereas *O. megalodon* predominates in all Middle Miocene to Pliocene deposits (Carrillo-Briceño et al., 2016a, 2016b; Perez et al., 2019; Perez, 2022).

Family Lamnidae Müller and Henle, 1838
Genus *Cosmopolitodus* Glikman, 1964
Cosmopolitodus hastalis (Agassiz, 1838)
(Fig. 6A–D)

Fig. 5. Lower lateral tooth of the otodontid lamniform *Otodus chubutensis* (Ameghino, 1901) (MUSM 5297) from the Early Miocene phosphorites of the Tunga Formation at Cerro Tiza (Ica Desert, Peru). Tooth is figured in lingual (1), labial (2), and profile (3) views. Scale bar = 20 mm.

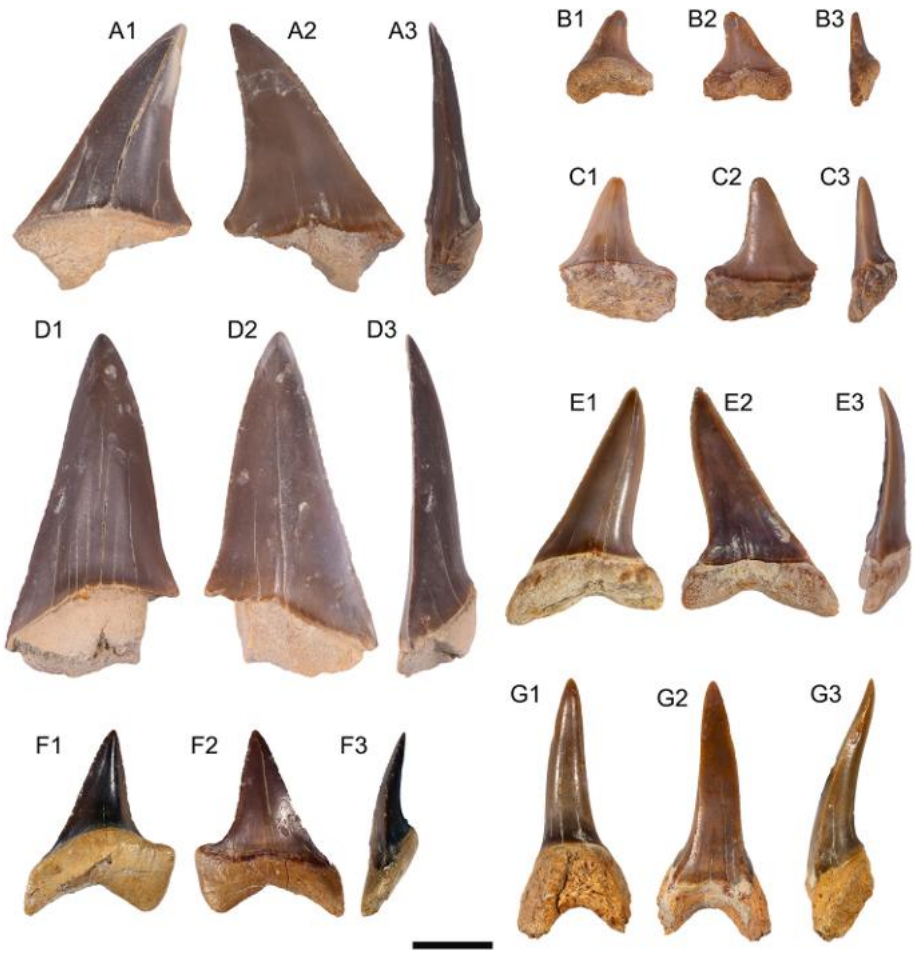

Fig. 6. Lamniformes from the Early Miocene phosphorites of the Tunga Formation at Cerro Tiza (Ica Desert, Peru). A, *Cosmopolitodus hastalis* (Agassiz, 1838) (MUSM 5298), upper lateral tooth; B, *Cosmopolitodus hastalis* (Agassiz, 1838) (MUSM 5299), upper posterior tooth; C, *Cosmopolitodus hastalis* (Agassiz, 1838) (MUSM 5300), lower posterior tooth; D, *Cosmopolitodus hastalis* (Agassiz, 1838) (MUSM 5301), lower anterior tooth; E, *Isurus oxyrinchus* Rafinesque, 1810 (MUSM 5302), upper anterior tooth; F, *Isurus oxyrinchus* Rafinesque, 1810 (MUSM 5303), upper lateral tooth; G, *Isurus oxyrinchus* Rafinesque, 1810 (MUSM 5304), lower anterior tooth. All teeth are figured in lingual (1), labial (2), and profile (3) views. Scale bar = 10 mm.

Material. 190 moderately preserved teeth, including MUSM 5298 (Fig. 6A), MUSM 5299 (Fig. 6B), MUSM 5300 (Fig. 6C) and MUSM 5301 (Fig. 6D).

Description. The examined material includes teeth representing most tooth positions. Their roots are lacking or incompletely preserved at best, and as such, they cannot be described properly. These teeth are large, the tallest crown reaching 40 mm in total height, suggesting a total tooth height around 50 mm. Based on these tooth sizes, following Landini et al. (2019), we hypothesize that the teeth of *C. hastalis* from Cerro Tiza belong to both juvenile and mature (adult) individuals.

The cusp of upper anterior teeth (Fig. 6A) is tall, symmetrical and slightly inclined distally, with sharp, smooth cutting edges. The labial face is flat, whereas the lingual face is strongly convex. The upper anterolateral and lateral teeth (Fig. 6B) become progressively more inclined distally, and display wider, more triangular crowns with convex mesial cutting edges. No serrations or lateral cusplets were observed.

The lower anterior teeth (Fig. 6D) are high and nearly symmetrical, with an equilateral triangular shape. The labial face is flat to weakly convex transversely, slightly overhanging the root with a concave bulge medially, whereas the lingual face is evenly convex and bears a faint lingual bulge near the crown base. The cutting edges are smooth and complete, extending from the apex to the crown-root junction. The lower lateral teeth (Fig. 6C) exhibit progressively broader and more distally inclined crowns. The cusp becomes shorter and wider, forming a distally recurved profile with an expanded crown base. The labial surface remains smooth and gently convex, while the lingual face becomes more swollen, producing a gently sigmoidal profile in lateral view. The distal cutting edge forms a broad, convex margin toward the distal heel, which is not distinct but merges smoothly with the crown margin. Lateral cusplets are absent throughout the series.

Remarks. The taxonomic history of *C. hastalis* has been long and complex, reflecting its intermediate morphology between the slender-toothed *Isurus* species and the broad-crowned *Carcharodon* lineage (see Maisch et al., 2025). Traditionally, all large, smooth-edged lamnid teeth from Neogene marine deposits were attributed to *Isurus hastalis* (Agassiz, 1838). Subsequent works, however, recognized that the teeth of *C. hastalis*, compared to those of other known species belonging to the genus *Isurus* Rafinesque, 1810, display some major differences, such as a significantly larger size and wider, less twisted crowns in the anterior teeth (Cappetta, 2012). This led several authors to propose alternative taxonomic interpretations over time. Glikman (1964) assigned this species to the then-new genus *Cosmopolitodus* in order to better reflect the putative phylogenetic affinities between this fossil taxon and the extant great white shark, *Carcharodon carcharias*. Glikman's (1964) hypothesis was subsequently supported by Muizon and de DeVries (1985) and Nyberg et al. (2006) among others. More recently, Ehret et al. (2012) even assigned *C. hastalis* to the genus *Carcharodon*, arguing that the former represents a direct ancestor of *C. carcharias* (Linnaeus, 1758). According to their hypothesis, the evolutionary transition toward the fully serrated cutting edges of *C. carcharias* would have occurred

through an intermediate form of Messinian age (7.25–5.33 Ma), namely, *Carcharodon hubbelli*, which exhibits a dentition similar to that of *C. hastalis* but with incipient marginal crenulations along the cutting edges. This evolutionary scenario has been adopted in most subsequent studies (e.g., Villafaña et al., 2020), yet authors such as Cappetta (2012), Collareta et al. (2017) and Landini et al. (2017a) have opted for retaining the species within the genus *Cosmopolitodus* Glikman, 1964. *Cosmopolitodus hastalis* is common worldwide in temperate to tropical neritic deposits of Early Miocene to Pleistocene age (Cappetta, 2012; Ebersole et al., 2017; Landini et al., 2019; Malyshkina et al., 2024).

Genus *Isurus* Rafinesque, 1810

Isurus oxyrinchus Rafinesque, 1810

(Fig. 6E–G)

Material. 216 moderately preserved teeth, including MUSM 5302 (Fig. 6E), MUSM 5303 (Fig. 6F), and MUSM 5304 (Fig. 6G).

Description. The examined material referred to the shortfin mako, *I. oxyrinchus*, comprises teeth representing most of the tooth positions. The teeth are medium-sized, with the largest specimen reaching up to approximately 40 mm in total height. Based on this maximum tooth size, and following Landini et al. (2019), we hypothesize that the teeth of *I. oxyrinchus* from Cerro Tiza belong to both immature and mature (adult) individuals.

The upper anterior teeth (Fig. 6E) are slightly larger than the lowers and have slenderer, distally inclined cusps that are more compressed labiolingually. The labial face is nearly flat, whereas the lingual face is convex. Upper lateral teeth (Fig. 6F) are increasingly inclined distally, showing the typical lamnid gradient in crown inclination. The enameloid is completely smooth. The cusp is narrow, with smooth cutting edges, and the crown maintains flat labial and convex lingual surfaces. The distal cutting edge forms a continuous curve without a defined heel. No serrations or lateral cusplets are present. The root is well developed and bears a wide basal furrow. The lower anterior teeth (Fig. 6G) are high and narrow, with an erect to slightly distally inclined cusp that is slender and sharply pointed. The crown is labiolingually compressed, with a flat to slightly convex labial face that slightly overhangs the root and has no labial bulge, and a strongly convex lingual face. The enameloid is completely smooth on all teeth. The cutting edges are smooth and do not reach the base of the crown. Lateral cusplets are absent. In profile view, the crown bends lingually and the cutting edges are slightly sigmoid in shape. The root is stout, with well-separated but almost vertical lobes and a pronounced lingual torus that bears a nutritive groove with a large central foramen. Lower anterolateral and lateral teeth possess broader crowns and are more distally inclined than the anterior ones. The labial face remains smooth and flat, while the lingual face becomes strongly convex, producing a weakly sigmoidal profile in lateral view. The crown is distally bent and the cutting edges are smooth, reaching the base of crown. Lateral cusplets are absent. The root lobes are more widely separated than in the anterior teeth.

Remarks. The taxonomic history of *Isurus oxyrinchus* has been complex, reflecting the longstanding difficulty of separating fossil lamnid taxa on the basis of isolated teeth. Historically, many Neogene lamnid teeth with smooth cutting edges were generically referred to *Isurus*, often without clear distinctions between *I. oxyrinchus*, *I. paucus*, and various fossil forms traditionally grouped under "*Isurus*" *hastalis*. Earlier works tended to treat all smooth-edged lamnid morphotypes as members of *Isurus*, whereas later revisions have refined this assignment based on crown proportions and curvature, and root morphology. As noted by Cappetta (2012), Collareta et al. (2017) and Landini et al. (2017a), the modern shortfin mako (*I. oxyrinchus*) is now regarded as distinct at the genus-level from the broad-crowned *Cosmopolitodus/Carcharodon* lineage. The diagnostic combination of narrow, labiolingually compressed, smooth-edged, sigmoid crowns lacking lateral cusplets and roots bearing a prominent lingual torus has been consistently recognized across Oligocene and Neogene deposits from North and South America, Japan, Africa and Europe (Cappetta, 2012; Höltke et al., 2024). These features have been used to separate *Isurus oxyrinchus* from both the extinct "*I.* *hastalis* complex, now generally placed within *Cosmopolitodus/Carcharodon*, as well as from *I. paucus*, whose teeth are more robust and less recurved. As a final note, Neogene fossil teeth nowadays usually assigned to *Isurus oxyrinchus* may once have been referred to the now obsolete name of *I. desori* (e.g., Purdy et al., 2001; Reinecke et al., 2011). However, despite small differences involving the size and length of the cutting edge, they are typically assigned to the *I. oxyrinchus* lineage.

Order Carcharhiniformes Compagno, 1973

Family Hemigaleidae Hasse, 1879

Genus *Hemipristis* Agassiz, 1834

Hemipristis serra (Agassiz, 1834)

(Fig. 7A and B)

Material. Nine teeth, including MUSM 5305 (Fig. 7A) and MUSM 5306 (Fig. 7B).

Description. The teeth of the snaggletooth shark, *Hemipristis serra*, display a pronounced heterodonty, both monognathic and dignathic.

Upper teeth such as the anterolateral figured in Fig. 7A are mesiodistally broad and labiolingually compressed, with a triangular, distally inclined crown that bears serrated cutting edges. The mesial cutting edge becomes distinctly convex toward the apex and is incised by numerous marked serrations that stop at a short distance from the tip of the crown. Conversely, the distal edge is markedly concave, and more robustly and strongly serrated; here again, serrations stop at a short distance from the tip of the crown. The labial face of the crown is flat to weakly convex, whereas the lingual face is strongly convex and overhangs the massive root. In profile view, the cusp is nearly straight or slightly bent lingually.

The only collected lower anterior tooth consists of a slender and symmetrical cusp that is almost vertically oriented in labial view. The labial crown face is slightly convex and slightly overhangs the root, whereas the lingual face is more convex and displays a faint basal swelling. In profile view, the crown strongly bends lingually. The smooth cutting edges are only present near the tip.

The lower lateral teeth (Fig. 7B) differ markedly from their upper counterparts, being more gracile and erect, with a narrow, high cusp and less developed serrations. The crown is elongated, with smooth or minutely serrated cutting edges that converge toward an acute apex without reaching it. The mesial edge is gently convex, whereas the distal edge is weakly concave near the base. The labial face is nearly flat, while the lingual face is convex, with a subtle median ridge. In lateral view, the cusp is slightly sigmoid, bending lingually near the apex.

Remarks. *Hemipristis serra* is an extinct congener of the extant snaggletooth shark, *H. elongata* (Klunzinger, 1871). It is widely distributed throughout the Neogene and Pleistocene shallow-marine deposits of the Atlantic, Pacific and Indo-West Tethys realms (Purdy et al., 2001; Cappetta, 2012; Landini et al., 2017a; Maisch et al., 2025). Its dentition is readily distinguished from that of *H. elongata* by the larger size and broader crowns of the upper teeth, the latter featuring coarser, more irregular serrations (Maisch et al., 2025). Thus, several authors recognize *H. serra* as a valid species of *Hemipristis*, a genus that reflects a rather conservative but distinctive lineage that persisted with little morphological modification since the Early Miocene, although some analyses highlighted a phyletic trend through the Miocene, involving an increase in tooth size and a progressive extension of the distal serrations, consistent with gradual morphological change rather than strict morphological stasis (Chandler et al., 2006).

Family Galeocerdonidae Poey, 1875

Genus *Galeocerdo* Müller and Henle, 1837

Galeocerdo cf. *aduncus* (Agassiz, 1834)

(Fig. 7C)

Material. Two fragmentary teeth, including MUSM 5307 (Fig. 7C).

Description. The specimen MUSM 5307 (Fig. 7C) represents an isolated distal heel, which is high and rather long, and bears large serrations in the form of five or six cusplets decreasing in size distally. The fragment also comprises part of the root in the lingual side.

Remarks. Due to their incompleteness, it is difficult to find

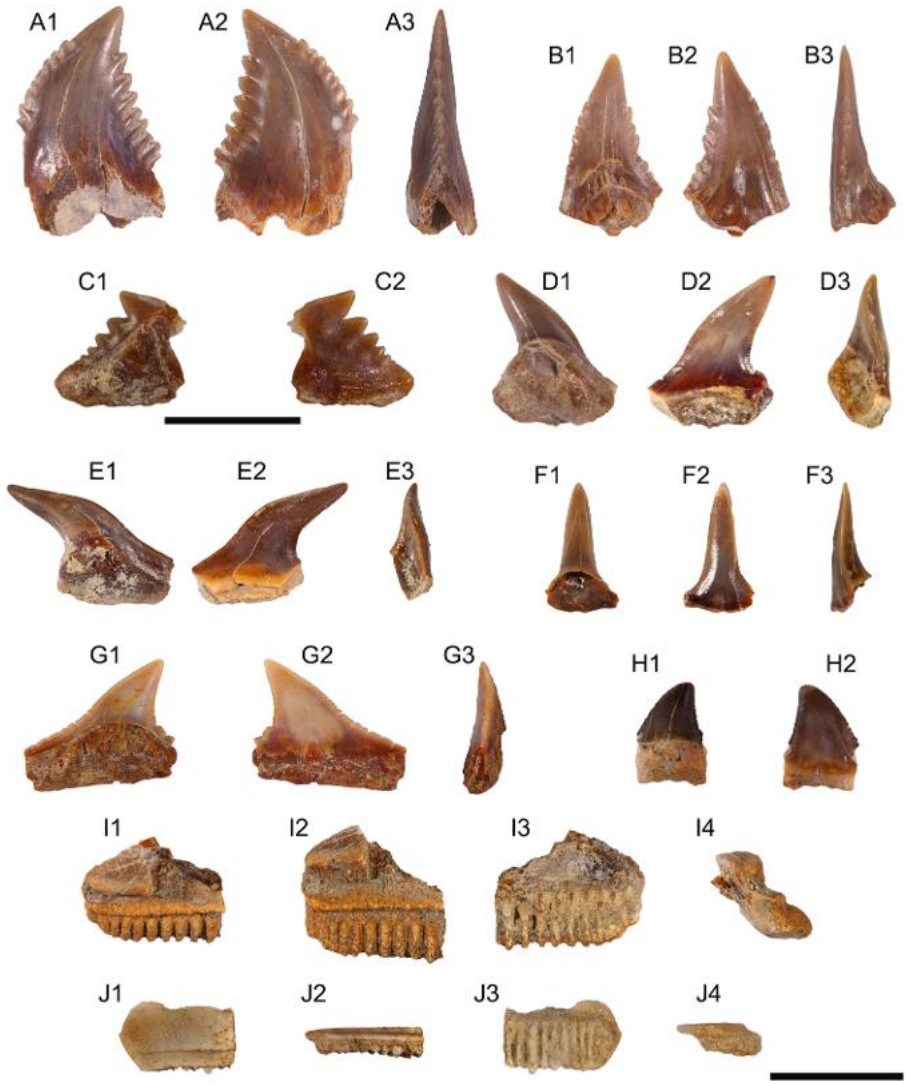

Fig. 7. Carcharhiniformes and Myliobatiformes from the Early Miocene phosphorites of the Tunga Formation at Cerro Tiza (Ica Desert, Peru). A, *Hemipristis serra* (Agassiz, 1834) (MUSM 5305), upper anterolateral tooth; B, *Hemipristis serra* (Agassiz, 1834) (MUSM 5306), lower lateral tooth; C, *Galeocerdo* cf. *aduncus* (Agassiz, 1834) (MUSM 5307), part of a distal heel and root lobe; D, *Physogaleus contortus* (Gibbes, 1849) (MUSM 5308), lower antero-lateral tooth; E, *Physogaleus contortus* (Gibbes, 1849) (MUSM 5309), lower lateral tooth; F, *Negaprion* cf. *brevirostris* (Poey, 1868) (MUSM 5310), lower anterior tooth; G, *Carcharhinus brachyurus* (Günther, 1870) (MUSM 5311), upper antero-lateral tooth; H, *Carcharhinus* cf. *leucas* (Valenciennes, 1839) (MUSM 5312), upper lateral tooth; I, *Aetobatus* sp. (MUSM 5313); J, *Rhinoptera* sp. (MUSM 5314). In images A to H teeth are figured in lingual (1), labial (2), and profile (3) views; in images I and J teeth are figured in occlusal (1), labial (2), basal (3) and profile (4) views. Scale bars A, B, D–J = 10 mm; C = 5 mm.

unambiguous characters to identify these specimens at the species level. However, being *Galeocerdo aduncus* the only true tiger shark species recovered in the Miocene deposits of Pacific South America (Cappetta, 2012; Landini et al., 2017a, 2019; Carrillo-Briceño et al., 2020; Collareta et al., 2021a), we are rather confident in referring these specimens to *G. aduncus*. The traits described for the distal heel, in particular, allow to exclude their assignment to the Middle Miocene to Recent *G. cuvier* as well as to the extinct *G. mayumbensis* (having more numerous, smaller cusplets along the distal heel) and *Physogaleus contortus* (which has more twisted cutting edges of the main cusp and lower cusplets on the distal heel) (see, e.g., Cappetta, 2012).

Genus *Physogaleus* Cappetta, 1980

Physogaleus contortus (Gibbes, 1849)

(Fig. 7D and E)

Material. 34 teeth, including MUSM 5308 (Fig. 7D) and MUSM 5309 (Fig. 7E).

Description. The anterior and anterolateral teeth feature a tall and strongly sigmoid main cusp that is compressed labiolingually and bent distally (Fig. 7D). The cutting edges are continuous, smooth at the crown apex and minutely serrated toward the base. The labial crown face is flat to slightly convex, overhanging the root with a rounded shoulder, whereas the lingual face is convex and bears a faint medial bulge. The mesial cutting edge is convex and twisted lingually, giving rise to the characteristic "contorted" appearance of the crown. The distal heel is short and concave and there is a notch separating the main cusp from the distal heel.

More lateral teeth (Fig. 7E) are slightly broader and display a more distally directed cusp. The mesial cutting edges become progressively longer and more twisted. The cusp exhibits fine, irregular serrations along the cutting edges. The root of more posterior teeth is bilobate, low and compact, the lobes being widely separated from each other by a narrow central groove that bears a large foramen.

The upper and lower teeth are similar in shape, although the upper teeth usually exhibit wider cusps.

Remarks. *Physogaleus contortus* has often been regarded as an extinct relative of *Galeocerdo*, and sometimes even as representing intraspecific

variation within *Galeocerdo aduncus* (see, e.g., Cappetta, 1987), yet it is now commonly retained in its own genus, *Physogaleus*, based on a slender, finely serrate crown, absence of large serrations on the distal heel, absence of a distinct notch separating the distal cutting edge from the distal heel, and thicker, more prominent lingual protuberance (Kent, 2018), all these features being absent in living and fossil *Galeocerdo* species. Stratigraphically, *P. contortus* ranges from the Oligocene to the Upper Miocene, with numerous Lower to Middle Miocene occurrences from Europe and the Americas (Reinecke et al., 2011; Cappetta, 2012; Carrillo-Briceño et al., 2019). *Physogaleus contortus* often lived sympatrically with *Galeocerdo aduncus*, but showing shifting relative abundances through time, being more common in Lower Miocene horizons at some Peruvian localities (Landini et al., 2017b, 2019; Villafaña et al., 2020; Maisch et al., 2025).

Family Carcharhinidae Jordan and Evermann, 1896

Genus *Negaprion* Whitley, 1940

Negaprion cf. *brevirostris* (Poey, 1868)

(Fig. 7F)

Material. MUSM 5310, a single partially preserved tooth (Fig. 7F).

Description. A single tooth cusp is identified as a lower anterior of *Negaprion brevirostris* based on the following combination of traits: the crown is high, broad and slightly compressed labiolingually, forming a symmetrical, triangular cusp; the cusp is erect, tapering gradually into a sharp, non-serrated apex; the cutting edges are continuous and almost smooth, and the crown-root junction is neat and gently concave in labial view. In profile view, the tooth is slightly bent lingually, with the crown leaning gently backward from the root. The enameloid surface is smooth and glossy, without striations or ornamentation.

Remarks. Teeth of *Negaprion brevirostris* differ from those of other sympatric requiem sharks, such as *Carcharhinus*, by their broader crown base, more erect cusp, and smooth or very finely serrated cutting edges (Cappetta, 2012; Perez et al., 2017). The labial crown face is less convex and lacks the basal bulge that is typical of *Carcharhinus* spp. Fossil teeth of *Negaprion* from the Neogene of North and South America (e.g., Carrillo-Briceño et al., 2015b; Landini et al., 2017a, 2019; Perez et al., 2017; Maisch et al., 2025) closely match those of the extant species, *N. brevirostris*, indicating long-term morphological conservatism within the genus since the Early Miocene. Other authors traditionally assigned Miocene occurrences of *Negaprion* to the extinct species *N. eurybathrodon* (e.g., Cappetta, 1987; Purdy et al., 2001; Aguilera et al., 2017). However, Pimiento et al. (2013) has shown that the Miocene morphology matches that proper of *N. brevirostris* and accordingly transferred those records to the extant species.

Genus *Carcharhinus* Blainville, 1816

Carcharhinus brachyurus (Günther, 1870)

(Fig. 7G)

Material. Six upper teeth, including MUSM 5311 (Fig. 7G).

Description. The upper teeth of the copper shark, *Carcharhinus brachyurus*, are up to 10 mm high in our sample. They have a broad, triangular crown that is almost straight in the anterior files and becomes progressively inclined in lateral positions. The labial face is flat and lacks a basal bulge; the lingual face is gently convex. The cutting edges are serrated; serrations are fine to incipient near the apex, becoming more pronounced along the mesial and distal heels. The heels are subrectilinear to slightly convex. In the best preserved specimens, the cusp is clearly separated from both heels. The root is relatively flat and bilobate, with a high basal face and a distinct lingual nutritive furrow. The root lobes form an obtuse angle that tightens in anteriormost positions (around 145°) and progressively opens toward the rear of the mouth, approaching 180° in the posteriormost files.

Remarks. The combination of a narrow, distally inclined crown with fine, apically diminishing serrations and a robust, bilobate root with a pronounced lingual groove is consistent with published descriptions of anterolateral upper teeth of *Carcharhinus* (e.g., Cappetta, 2012). Furthermore, the studied specimens are particularly close to *C. brachyurus* in having fine serrations that become coarser on the heels and a somewhat truncated main cusp (Purdy et al., 2001). Along the Pacific margin of South America, *C. brachyurus* occurs from central Chile northward to Ecuador (Carrillo-Briceño et al., 2013, 2014). In Peru, occurrences of this species are documented in sedimentary units dating back from the Lower Miocene through the Lower Pliocene (Landini et al., 2017a, 2017b).

Carcharhinus cf. *leucas* (Valenciennes, 1839)

(Fig. 7H)

Material. MUSM 5312, a single fragmentary tooth (Fig. 7H).

Description. The specimen represents the main cusp of an upper lateral tooth. The crown is broad, triangular, slightly inclined distally, with a sturdy appearance. Serrations along the cutting edges are coarse, uniform, and persist toward the apex.

Remarks. The combination of characters above appears in our opinion consistent with description of *C. leucas* (see, e.g., Landini et al., 2017a; Maisch et al., 2025). By contrast, *C. brachyurus* exhibits a narrow-cusped pattern that becomes progressively more inclined laterally, and its cutting edges bear finer serrations that are often incipient to absent near the apex, but strengthen on the heels (Landini et al., 2017a; Maisch et al., 2025). However, due to the fragmentary nature of the specimen, its identification as *Carcharhinus leucas* is only tentative. In any case, occurrences of *C.* cf. *leucas* have been already reported from the Miocene of Peru and other localities of the South America (e.g., Carrillo- Briceño et al., 2019; Landini et al., 2019).

Carcharhinus sp.

Material. 14 incomplete teeth.

Description. Although these teeth unquestionably exhibit diagnostic characters of the genus (see, e.g., Cappetta, 2012), their fragmentary nature prevents taxonomic identification at the species level.

Superorder Batomorphii Cappetta, 1987

Order Myliobatiformes Compagno, 1973

Family Aetobatidae Agassiz, 1858

Genus *Aetobatus* Blainville, 1816

cf. *Aetobatus* sp.

(Fig. 7I)

Material. MUSM 5313, a single partially preserved tooth (Fig. 7I).

Description. This single specimen consists of a fragmentary tooth. The crown is relatively high, roughly equal to the root height. The crown labial surface is convex and overhangs the root. The crown surface displays fine wrinkles. The tooth is labiolingually thicker in the central region than at the lateral end, reflecting the central strengthening of the occlusal surface for crushing function. The lingual bulge is well marked.

The root is well developed and polyaulacorhizous, consisting of numerous, thin, vertically oriented lamellae separated by shallow nutritive grooves that produce a comb-like appearance. In labial/lingual view, its height decreases toward the lateral edge. In profile view, the root is conspicuously displaced lingually, extending well posterior to the crown.

Remarks. Despite the fragmentary nature of the specimen, this tooth might be tentatively referred to the Pacific eagle ray genus *Aetobatus* due to its root being conspicuously displaced lingually relative to the crown, a trait that is absent or way less marked in other eagle ray genera such as *Myliobatis* and *Aetomylaeus* as well as in the cownose ray genus *Rhinoptera* (Cappetta, 2012; Ebersole et al., 2019; Maisch et al., 2025). However, the extreme incompleteness and high degree of intraspecific variation in dental morphology (e.g., Hovestadt and Hovestadt-Euler, 2013) make our assumption tentative and prevent any identification of this specimen to the species level. Our identification is nonetheless consistent with the South American Miocene fossil record of *Aetobatus*, since it includes occurrences from Chile, Ecuador, Peru and Venezuela (e.g., Long, 1993; Carrillo-Briceño et al., 2015b; Landini et al., 2017a).

Family Rhinopteridae Jordan and Evermann, 1896

Genus *Rhinoptera* Cuvier, 1829

Rhinoptera sp.

(Fig. 7J)

Material. MUSM 5314, a single partially preserved tooth (Fig. 7J).

Description. The incomplete tooth that we refer to as *Rhinoptera* sp. is broad and was originally characterised by an hexagonal outline, broader than long, with sharp lateral angles of approximately 90°, thus likely originating from a symphyseal position. In labial or lingual view, the crown appears as weakly convex. In occlusal view, the lingual and labial edges are roughly rectilinear, whereas the crown surface is covered with enameloid that exhibits a fine ornamentation consisting of a beaded texturing arranged in longitudinal rows. The labial and lingual crown faces are vertical and flat, and the labial face slightly overhangs the root. The crown base overhangs the root on the distal/mesial and labial sides, but not on the lingual margin.

The root is polyaulacorhizous, consisting of numerous parallel lamellae separated by nutritive grooves. The root is relatively low compared to the crown. In profile view, the root is slightly displaced lingually, and the root lamellae typically do not extend beyond the lingual crown foot.

Remarks. The combination of a flat ornamented occlusal surface, hexagonal shape with rectilinear labial and lingual edges, and polyaulacorhizous root structure typifies the crushing dentition characteristic of the cownose ray *Rhinoptera*. This mosaic of features easily distinguishes this taxon from *Aetomylaeus* and *Myliobatis*, which have concave labial and convex lingual faces, and a higher root. At the same time, the root that is not or only slightly displaced lingually relative to the crown excludes an assignment to the Pacific eagle ray genus *Aetobatus*, whose root is strongly displaced lingually (e.g., Cappetta, 2012; Maisch et al., 2025). Due to the difficulty of recognizing specific diagnostic characters, identification at the species-level is not possible.

Our identification is consistent with the South American Miocene fossil record of *Rhinoptera*, since the genus has been already recorded from several localities (e.g., Carrillo-Briceño et al., 2016; 2019).

4.4. Taxonomic composition

The overall taxonomic composition of the Early Miocene elasmobranch assemblage of the Tunga Formation at Cerro Tiza includes at least 17 species belonging to 15 genera in 11 families and three orders of elasmobranchs (Lamniformes, Carcharhiniformes and Myliobatiformes) (Table 1). At high taxonomic level, all the orders and most families (all but the Otodontidae) are still living today, and only four out of 15 genera are extinct. Of the 17 species, at least seven are extinct. Squalomorph sharks have not been recorded and, among the batoids, only the stingrays (Myliobatiformes) are present. Lamniforms are the most diverse and abundant sharks in the assemblage, including six families and nine species. Although the Alopiidae and the Carcharhinidae are the most represented sharks in terms of diversity, accounting as they do for three species, the Lamnidae are by far the most abundant, with *Cosmopolitodus hastalis* and *Isurus oxyrinchus* collectively representing some 76% of the material examined (Fig. 8; Table 2). Carcharhiniforms are represented by three families: the Carcharhinidae, which likely include two species of *Carcharhinus*, whereas *Negaprion* and *Physogaleus* are represented by a single species each. *Galeocerdo* and *Hemipristis* are the only representative of the families Galeocerdonidae and Hemigaleidae, respectively. Batoids are only represented by two stingray genera (*Rhinoptera* and cf. *Aetobatus*), both being known by a single specimen.

4.5. Sampling and taxonomic diversity

Table 3 shows the results of the Shareholder Quorum Subsampling (SQS) performed at the genus level. The total abundance (N) ranges from 62 to 3918 individuals for each site. The observed alpha-taxonomic richness (S obs) varies between 12 and 32 genera across the studied assemblages. The high Good's u values (>0.95) indicate high sample completeness in all assemblages (i.e., more than 95% of the taxa should be represented). The SQS richness values, defined as the number of taxa drawn before the quorum is reached, reveal differences in the frequency distribution and dominance of taxa across the assemblages. The lowest SQS value (0.99) of the Peruvian Late Miocene assemblage at Cerro Colorado (Landini et al., 2017a) indicates that a single dominant genus (*Carcharhinus*, mostly represented by a single species, *C. brachyurus*) contributes rapidly to the cumulative frequency, indicating high dominance, as also shown by the highest values of Dominance and Berger-Parker indices as well as by the lowest scores for the Simpson and Shannon indices. Conversely, the highest SQS value (3.36) of the Early Miocene Chilean assemblage (Villafaña et al., 2019) shows that several taxa contribute to reach the quorum as defined by Alroy (2010), indicating low dominance, as also shown by the lowest values of Dominance and Berger-Parker indices as well as by the highest scores for the Simpson and Shannon indices.

Intermediate values are observed for the remaining assemblages. In particular, the mid-low SQS value (1.89) of the Early Miocene assemblage of Cerro Tiza described here reveals that two lamniforms (*Cosmopolitodus hastalis* and *Isurus oxyrinchus*) contribute quite rapidly to the cumulative frequency, indicating a high level of dominance, as also confirmed by the other indices. However, this value needs to be treated cautiously in the light of the taphonomic signature of the site (see Discussion below).

4.6. Ecological affinities and paleobathymetric analysis

Although most of the elasmobranch species found at Cerro Tiza are benthopelagic (10 out of 17), the assemblage is apparently dominated by epipelagic lamniform sharks, with *Isurus oxyrinchus* and *Cosmopolitodus hastalis* representing the most abundant taxa (40.5% and 35.7% of the specimens, respectively) (Fig. 8; Table 1). The modern shortfin mako, *Isurus oxyrinchus*, is a pelagic-oceanic, oceanodromous species that, though able to occupy a broad bathymetric range, prefers depths around 100-150 m, particularly within neritic and epipelagic settings, whereas *Cosmopolitodus hastalis* might have preferred depths up to 250 m, if *Carcharodon carcharias* is considered as its closest relative (see, e.g., Ehret et al., 2012; Nyberg et al., 2006) (Fig. 9; Table 1). Overall, these data are broadly consistent with an inner to mid-shelf depositional environment for the Cerro Tiza paleobiotope. This interpretation is further supported by the presence of other lamniform taxa (e.g., *Alopias superciliosus*, *A. vulpinus*, *Pseudocarcharias kamoharai*) and carcharhiniforms (*Galeocerdo* cf. *aduncus*) that predominantly live in neritic-epipelagic habits, preferably at depths of 0–200 m according to their extant analogues (Fig. 9; Table 1).

Strictly shallow-water coastal benthopelagic taxa (e.g. *Carcharias*, *Carcharhinus*, *Hemipristis*, *Negaprion*, cf. *Aetobatus*, *Rhinoptera*) are sparsely represented. They collectively account for about 8.7% of the total sample, therefore suggesting the presence of neritic shallow habitats in the surrounding areas.

Mesobathyal indicators (*Mitsukurina* cf. *lineata*, preferring depth ranges between 270 and 960 m) are extremely rare and contribute only to a very minor fraction of the assemblage (<0.4%). They cannot define the paleoenvironment, but their presence might be considered as results of sporadic entry into the Cerro Tiza paleobiotope or as reworked material.

In conclusion, the assemblage features a strong representation of epipelagic and neritic taxa, whereas both very shallow-water and deep-water indicators are subordinate. Taken together, these occurrences are broadly consistent with an inner-to mid-shelf signal, but the condensed and reworked nature of the deposit prevents a more precise paleobathymetric reconstruction.

4.7. Dietary preferences

The dietary spectrum of the Early Miocene elasmobranch assemblage from Cerro Tiza is represented by four trophic categories: piscivorous, durophagous/cancritrophic, teuthitrophic and eurytrophic taxa (Table 1). These trophic assignments are intended as broad ecological categories inferred from dental morphology and extant congeners/

Table 1
Paleodiversity of the Early Miocene elasmobranch assemblage of Cerro Tiza (Tunga Formation; Ica Desert; Peru), with habitat and feeding preferences of the taxa, based on the biology of their extant relatives. Grey cells indicate the preferred feeding preference.

Order	Family	*Taxon*	Extant relative	Benthopelagic	Pelagic	Neritic/ epipelagic	Bathyal/meso-bathypelagic	Bathymetric depth (m)	Preferred range (m)	Piscivorous	Durophagous/ cancritrophic	Teuthitrophic	Eurytrophic	Trophic level	Sources
Lamniformes	Mitsukurinidae	*Mitsukurina* cf. *lineata*	*Mitsukurina owstoni*	X		X	X	30-1300	270-960	X	X	X		4.1	a
	Alopiidae	*Alopias superciliosus*	*Alopias superciliosus*		X	X	X	0-730	0-100	X		X		4.2-4.5	a, b
		Alopias vulpinus	*Alopias vulpinus*		X	X	X	0-650	0-200	X	X	X		4.2-4.5	a, b
		Anotodus retroflexus			X	X		?	?	X		X	X	~4.3	c, d
	Pseudocarchariidae	*Pseudocarcharias* sp.	*Pseudocarcharias kamoharai*		X	X	X	0-590	0-200	X		X		4.5	a
	Carchariidae	*Carcharias taurus*	*Carcharias taurus*	X		X		1-191	15-25	X	X	X		4.4-4.5	a, b
	Otodontidae	*Otodus chubutensis*			X	X	X	?	?	X			X	5.7-7.6	c, e
	Lamnidae	*Cosmopolitodus hastalis*	*Carcharodon carcharias*		X	X	X	0-1280	0-250	X			X	4.5-6.0	a, d, e
		Isurus oxyrinchus	*Isurus oxyrinchus*		X	X	X	0-888	100-150	X		X	X	4.3-5.4	a, b
Carcharhiniformes	Hemigaleidae	*Hemipristis serra*	*Hemipristis elongata*	X		X		1-130	?	X		X		4.3-4.5	a, b
	Galeocerdonidae	*Galeocerdo* cf. *aduncus*	*Galeocerdo cuvier*	X		X	X	0-800	0-140	X	X	X	X	3.8-5.0	a, b, f
		Physogaleus contortus			X	X		?	?	X		X		~4.2	d, g
	Carcharhinidae	*Negaprion* cf. *brevirostris*	*Negaprion brevirostris*	X		X		0-92	?	X				4.2-4.5	a, b
		Carcharhinus brachyurus	*Carcharhinus brachyurus*	X		X	X	0-360	0-100	X		X		4.2-4.5	a, b
		Carcharhinus cf. *leucas*	*Carcharhinus leucas*	X		X		1-164	1-30	X	X	X	X	4.3	a, b
		Carcharhinus sp.	*Carcharhinus* spp.	X		X	X	0-360	0-100	X	X	X	X	4.2-4.5	a, b
Myliobatiformes	Aetobatidae	cf. *Aetobatus* sp.	*Aetobatus* spp.	X		X		1-100	20-25	X	X	X		3.6-4.2	a
	Rhinopteridae	*Rhinoptera* sp.	*Rhinoptera* spp.	X		X		0-65	0-25	X	X			3.2-4.2	a

Sources: a) Froese and Pauly (2025); b) Cortés (1999); c) Carrillo-Briceño et al. (2019); d) Kast et al. (2022); e) Landini et al. (2019); f) Dicken et al. (2017); g) Carrillo-Briceño et al. (2016).

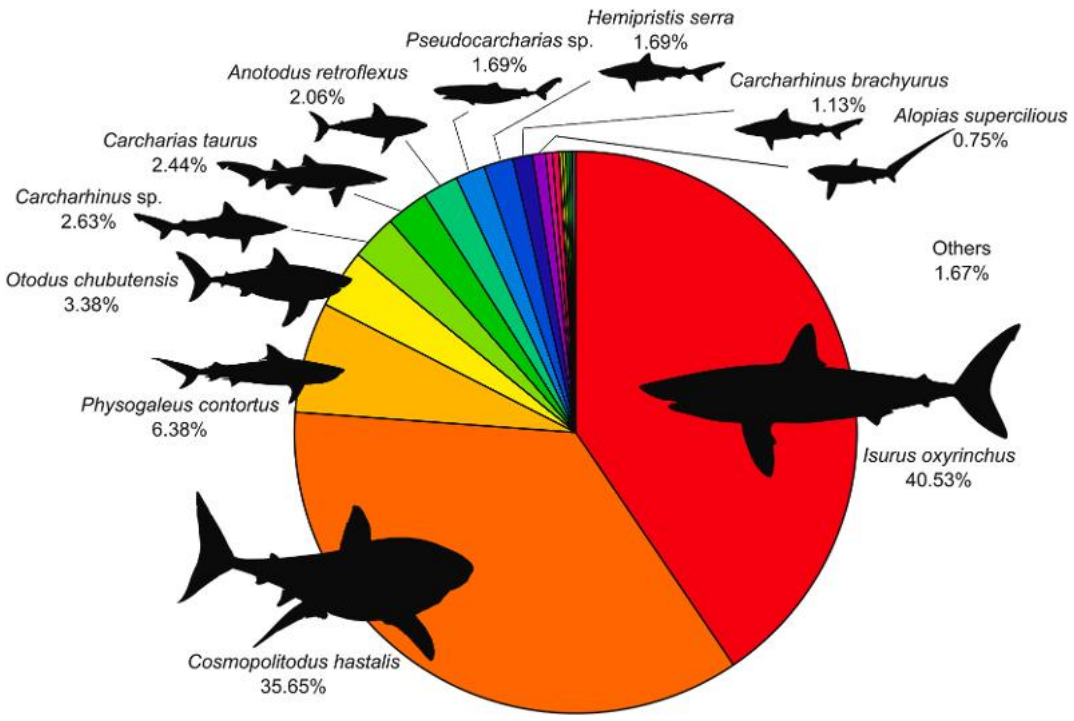

Fig. 8. Pie chart showing the relative abundance of the Early Miocene elasmobranchs recovered at Cerro Tiza (Tunga Formation, Ica Desert, Peru). Silhouettes are from PhyloPic (free silhouette images of life forms; https://www.phylopic.org/).

confamilials, and should not be interpreted as detailed species-level dietary reconstructions. Piscivorous species are the most represented trophic group in terms of diversity (70.6% of species) and abundance (57.7% of individuals), with *Isurus oxyrinchus* alone representing about 40.5% of the total assemblage. We included in this count also the extinct pelagic alopiid *Anotodus retroflexus* and the carcharhinid *Physogaleus contortus*, since their tearing or cutting dental type suggest a fish-based diet (see, e.g., Cappetta, 2012).

Three out of 17 species (17.7%) were primarily eurytrophic predators, representing the second most important trophic group in terms of diversity and abundance (39.4%), with *Cosmopolitodus hastalis* alone representing about 35.7% of the total assemblage.

Primarily durophagous/cancritrophic taxa include only indeterminate species of the stingrays *Aetobatus* and *Rhinoptera*, this trophic group representing about 17.8% of the species but less than 0.4% in terms of abundance.

There are no microphagous filter feeders (diet based mainly on plankton) or exclusively teuthitrophic species in the Cerro Tiza assemblage, although modern representatives of *Alopias* can integrate their diet with cephalopods (squid and cuttlefish) or even mostly feed on them in some populations (e.g., Cortés, 1999; Froese and Pauly, 2025).

4.8. Faunal comparisons

Along the Pacific coast of South America, a single taxon (*Isurus oxyrinchus*) is present in at least six Miocene assemblages, while at least four species (*Cosmopolitodus hastalis*, *Carcharhinus brachyurus*, *Galeocerdo aduncus* and *Physogaleus contortus*) being recorded in four marine deposits of Peru, Chile and Ecuador (Table 2) (Landini et al., 2017a, 2019; Villafaña et al., 2019; Carrillo-Briceño et al., 2020; Chávez-Hoffmeister and Villafaña, 2023). Many such taxa have been found in other early Neogene deposits worldwide (e.g., Cappetta, 2012), corroborating their cosmopolitan distribution during the Miocene.

The taxonomic similarity analysis based on the Dice index shows that the strongest taxonomic affinities of the Early Miocene elasmobranch assemblage from Cerro Tiza are with two other Peruvian assemblages (Table 4), namely, the Upper Miocene Cerro Colorado assemblage of the Pisco Formation (Dice correlation index 0.733), and the Lower Miocene Zamaca locality of the Chilcatay Formation (0.688). A low-intermediate taxonomic similarity is also retrieved with the Oligo-Miocene Montañita-Olón assemblage from the Dos Bocas Formation of Ecuador (0.486). In contrast, the Cerro Tiza assemblage shares only very limited similarity with the Middle Miocene to Pliocene assemblage of the Bahía Inglesa Formation at Los Dedos, Chile (0.340) and with the Lower Miocene localities from Chile (0.222). No shared taxa were detected between the Lower Miocene Cerro Tiza assemblage and the Upper Miocene Econssa locality of the Bahía Inglesa Formation of Chile (0.000). Overall, these values indicate that the Cerro Tiza assemblage shows its strongest taxonomic similarities within Peru, while its faunal similarity with assemblages from Ecuador and Chile is progressively lower, down to no affinities with the younger Chilean Econssa fauna.

These results are corroborated by the cluster analysis based on the Dice similarity index (Fig. 10), which provides a consistent visual representation of the observed faunal relationships.

Being the relative abundance of the taxa likely biased by taphonomic filtering (see Discussion below), we did not perform any analysis to test the ecological similarity based on the abundance of dominant taxa.

5. Discussion

5.1. Taphonomic remarks

Investigating the petrographic, mineralogical and chemical composition of the Middle to Upper Miocene phosphorite layers of the Pisco Formation, Bosio et al. (2024) emphasized several aspects of the sedimentary regime that are crucial for understanding the elasmobranch assemblage reported here. Phosphorites accumulate where phosphate precipitation is confined to the upper few cm of the sediment column (i.e., the zone of phosphogenesis) and grains have a long residence time near the sediment-water interface (Pufahl and Grimm, 2003). Low net sedimentation rates and repeated reworking/winnowing cycles are therefore integral to phosphate grain formation and concentration

Table 2
Genus-level elasmobranch-tooth abundances of the Miocene elasmobranch assemblage of South America used for comparisons. Values represent % of individuals per assemblage.

Superorder	Order	Family	*Genus*	Peru			Ecuador	Chile		
				Early Miocene - Cerro Tiza (Tunga Fm)	Early Miocene - Zamaca (Chilcatay Fm) (a)	Late Miocene - Cerro Colorado (Pisco Fm) (b)	Oligo/ Miocene Montañita-Olón (Dos Bocas Fm) (c)	Early Miocene Navidad, Ranquil and Lacui Fms (d)	Mid Miocene - Pliocene Los Dedos (Bahia Inglesa Fm) (e)	Late Miocene Econssa (Bahia Inglesa Fm) (f)
Squalomorphi	Hexanchiformes	Heptranchidae	*Heptranchias*	0	0	0	7.07	0	0	0
		Hexanchidae	*Hexanchus*	0	0	0	7.83	0	2.92	0
			Notorynchus	0	0	0	0	0	0.15	0
	Echinorhiniformes	Echinorhinidae	*Echinorhinus*	0	0	0	0.25	0	0.22	0
			Paraechinorhinus	0	0	0	0.25	0	0	0
	Squatiniformes	Squatinidae	*Squatina*	0	0.05	0.05	0	12.90	6.22	4.74
	Pristiophoriformes	Pristiophoridae	*Pristiophorus*	0	0	0	5.81	8.06	3.07	0
			Pliotrema	0	0	0	0	0	0.07	0
			Pochitaserra	0	0	0	0	0	0	4.74
	Squaliformes	Centrophoridae	*Centrophorus*	0	0	0	11.62	0	0	0
		Dalatiidae	*Dalatias*	0	0	0	0.25	0	0.07	0
		Squalidae	*Squalus*	0	0	0	0	6.45	0	0
Galeomorphi	Heterodontiformes	Heterodontidae	*Heterodontus*	0	0	0	0	4.84	0.67	1.58
	Orectolobiformes	Brachaeluridae	*Brachaelurus*	0	0	0	0	0	0.07	0
			Eostegostoma	0	0	0	0	0	0.07	0
		Rhincodontidae	*Rhincodon*	0	0	0	0.25	0	0	0
	Lamniformes	Mitsukurinidae	*Mitsukurina*	0.38	0	0	2.27	0	0	0
		Alopiidae	*Alopias*	0.94	0.41	0	2.27	1.61	0	0
			Anotodus	2.06	0.92	0.03	0	0	0	0
		Pseudocarcharidae	*Pseudocarcharias*	1.69	0	0.08	0	0	0	0
		Cetorhinidae	*Cetorhinus*	0	0	0	0	0	3.15	2.63
		Megachasmidae	*Megachasma*	0	0.05	0	0	0	0.67	0
		Odontaspididae	*Odontaspis*	0	0	0	5.05	4.84	2.10	0
		Carchariidae	*Carcharias*	2.44	0.10	0.62	0.25	9.68	0.22	0
		Otodontidae	*Otodus*	3.38	1.53	0.29	1.26	0	8.55	0
			Carcharoides	0	0	0.03	0	0	0	0
			Megalolamna	0	0.03	0	0.76	0	0	0
			Parotodus	0	0.08	0	0.51	0	0.15	0
		Lamnidae	*Carcharodon*	0	0	0	0	0	15.37	0
			Carcharoides	0	0	0	0	30.65	0	0
			Cosmopolitodus	35.65	28.74	6.81	0	0	38.61	0
			Isurus	40.53	16.00	2.70	1.77	11.29	9.90	0
	Carcharhiniformes	Scyliorhinidae	*Megascyliorhinus*	0	0	0	0	6.45	0	0
		Triakidae	*Galeorhinus*	0	0	0	0	1.61	0.90	51.05
			Mustelus	0	0	0	0	1.61	0	1.05
			Triakis	0	0	0	0	0	0	1.05
		Hemigaleidae	*Hemipristis*	1.69	0.61	0	0.51	0	0	0
			Paragaleus	0	0	0	0	0	0.07	0
		Galeocerdonidae	*Galeocerdo*	0.38	5.16	0.83	3.28	0	0.15	0
			Physogaleus	6.38	10.97	0.13	3.03	0	0	0
		Sphyrnidae	*Sphyrna*	0	0.87	1.51	6.31	0	0.15	0
		Carcharhinidae	*Negaprion*	0.19	0.77	0.03	0	0	0	0
			Isogomphodon	0	0	0	0	0	0.07	0
			Prionace	0	0	0	0	0	0.15	0
			Carcharhinus	3.94	33.69	81.84	36.87	0	1.95	0
Batomorphii	Rajiformes	Arhynchobatidae	*Sympterygia*	0	0	0	0	0	0	4.21
		Rajidae	*Dipturus*	0	0	0	0	0	0	7.89
			Raja	0	0	0	0	0	0.15	18.95
	Rhinopristiformes	Pristidae	*Anoxypristis*	0	0.03	0	0	0	0	0
		Rhinobatidae	*Rhinobatos*	0	0	0	0	0	0	1.05
	Myliobatiformes	Dasyatidae	*Dasyatis*	0	0	0	0	0	0.07	1.05
		Aetobatidae	*Aetobatus*	0.19	0	0.05	0	0	0.45	0
		Myliobatidae	*Aetomylaeus*	0	0	0	0	0	0.90	0
			Myliobatis	0	0	5.01	0	0	2.55	0
		Rhinopteridae	*Rhinoptera*	0.19	0	0	0	0	0.15	0
		Mobulidae	*Mobula*	0	0	0	2.53	0	0	0

Sources: a) Landini et al. (2019); b) Landini et al. (2017a); c) Carrillo-Briceño et al. (2020); d) Chávez-Hoffmeister and Villafaña (2023); e) Villafaña et al. (2019); f) Villafaña et al. (2025).

(Föllmi et al., 1991). For vertebrates, this means that the EPB phosphorite lags might represent strongly time-averaged bonebeds where many generations of shed teeth and skeletal elements are concentrated into thin phosphatic layers (see, e.g, Martinez et al., 2025).

Phosphorites of the Pisco Formation are associated with wave ravinement and "dynamic sediment bypass" in the lower shoreface, with alternations of deposition and erosional winnowing by storms and currents (Bosio et al., 2024). In this context, large, thick-crowned, mechanically robust lamniform teeth such as those of *Isurus*, *Cosmopolitodus* and *Otodus* may have survived repeated episodes of exhumation,

Table 3
Results of the Shareholder Quorum Subsampling (SQS) and diversity indices of the Miocene South America elasmobranch assemblages, performed at genus level.

	Peru			Ecuador	Chile		
	Early Miocene - Cerro Tiza (Tunga Fm) (a)	Early Miocene - Zamaca (Chilcatay Fm) (b)	Late Miocene - Cerro Colorado (Pisco Fm) (c)	Oligo/Miocene Montañita-Olón (Dos Bocas Fm) (d)	Early Miocene Navidad, Ranquil and Lacui Fms of Chile (e)	Mid Miocene - Pliocene Los Dedos (Bahia Inglesa Fm) (f)	Late Miocene Econssa (Bahia Inglesa Fm) (g)
Number of specimens (N)	533	3918	3850	396	62	1334	190
α-diversity (S obs)	15	17	15	22	12	32	12
Good's u value	0.994	1.000	0.999	0.987	0.952	0.995	1.000
SQS richness value	1.889	2.071	0.991	3.086	3.362	2.435	1.075
Dominance D	0.299	0.237	0.678	0.173	0.139	0.198	0.307
Berger-Parker	0.405	0.337	0.818	0.369	0.307	0.386	0.511
Simpson 1-D	0.702	0.763	0.322	0.827	0.861	0.802	0.693
Shannon H	1.594	1.679	0.7762	2.297	2.237	2.159	1.663

Sources: a) Landini et al. (2019); b) Landini et al. (2017a); c) Carrillo-Briceño et al. (2020); d) Villafaña et al. (2019); e) Chávez-Hoffmeister and Villafaña (2023); f) Villafaña et al. (2025).

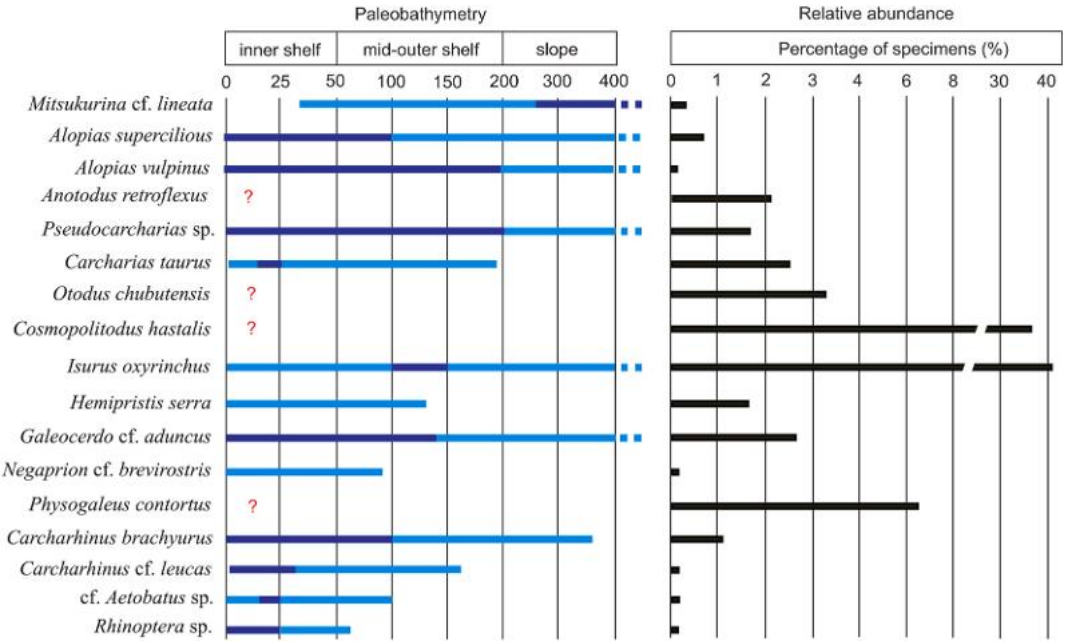

Fig. 9. Bathymetric ranges estimated for the Early Miocene taxa of Cerro Tiza based on the biology of their extant relatives, and their relative abundance. Dark blue indicates the preferred bathymetric range. Dashed lines indicate that the bathymetric range is greater. Question marks indicate that depth range for some extinct genera cannot be inferred, being difficult to closely relate them with any extant relative. In the relative abundance graph the y-axis is shortened between 8 and 30 to improve the values visualization; note the greater abundance of the pelagic lamnids *Isurus* and *Cosmopolitodus*. (For interpretation of the references to colour in this figure legend, the reader is referred to the Web version of this article.)

transport and abrasion. More delicate and/or smaller teeth, such as those of carcharhinids and batoids, and thin fish bones are more prone to fragmentation and dissolution, especially under suboxic to dysoxic conditions with intense microbial activity. Bosio et al. (2024) explicitly noted the occurrence of polished vertebrate bone fragments and shark teeth intimately associated with intraclasts and basement clasts in these lags of the Pisco Formation, highlighting the repeated reworking of the skeletal materials. The authors stressed that the microbial degradation of organic matter and the dissolution of fish debris at the seafloor are major sources of phosphorus to porewaters along the Peruvian upwelling margin (Bosio et al., 2024). This implies that a large fraction of fish hard parts is chemically "consumed" to promote phosphogenesis, rather than preserved as articulated skeletons or even as identifiable isolated bones. Practically, the large biomass of small schooling fishes that powered the food web and that would be the main diet of the piscivorous sharks mostly entered the lithosphere as fine phosphatic mud, not as recognizable fossil elements. In contrast, large, enameloid-coated shark teeth such as those of *Isurus* and *Cosmopolitodus* are resistant to dissolution and mechanically concentrated along with other phosphatic clasts. In this perspective, the processes that results in the accumulation of the phosphorite (namely, slow burial, suboxic porewaters, intense microbial activity and repeated winnowing) actively contributed to erase or pulverize much of the lower-trophic level fish record while concentrating the most robust teeth.

In conclusion, the dominance of a limited number of taxa within the Early Miocene Tunga phosphorite lag is best interpreted as the result of both ecological and taphonomic control. These large taxa were likely important components of the higher trophic structure represented in the studied assemblage, but the processes that led to the formation of the phosphorite layers likely amplified their representation relative to

Table 4
Taxonomic similarity analysis based on the Dice index showing taxonomic affinity among the Miocene South American elasmobranch assemblages.

	Early Miocene - Cetto Tiza (Tunga Fm) (this paper)	Early Miocene - Zamaca (Chilcatay Fm) (a)	Late Miocene - Cerro Colorado (Pisco Fm) (b)	Oligo/Miocene Montañita-Olón (Dos Bocas Fm) (c)	Early Miocene Navidad, Ranquil and Lacui Fms (d)	Mid Miocene - Pliocene Los Dedos (Bahia Inglesa Fm) (e)	Late Miocene Econssa (Bahia Inglesa Fm) (f)
Early Miocene - Cerro Tiza (Tunga Fm) (this paper)	1.000	0.688	0.733	0.486	0.222	0.340	0.000
Early Miocene - Zamaca (Chilcatay Fm) (a)	0.688	1.000	0.688	0.564	0.276	0.408	0.069
Late Miocene - Cerro Colorado (Pisco Fm) (b)	0.733	0.688	1.000	0.378	0.222	0.426	0.074
Oligo/Miocene Montañita-Olón (Dos Bocas Fm) (c)	0.486	0.564	0.378	1.000	0.294	0.444	0.000
Early Miocene Navidad, Ranquil and Lacui Fms (d)	0.222	0.276	0.222	0.294	1.000	0.318	0.333
Mid Miocene - Pliocene Los Dedos (Bahia Inglesa Fm) (e)	0.340	0.408	0.426	0.444	0.318	1.000	0.273
Late Miocene Econssa (Bahia Inglesa Fm) (f)	0.000	0.069	0.074	0.000	0.333	0.273	1.000

Sources: a) Landini et al. (2019); b) Landini et al. (2017a); c) Carrillo-Briceño et al. (2020); d) Villafaña et al. (2019); e) Chávez-Hoffmeister and Villafaña (2023); f) Villafaña et al. (2025).

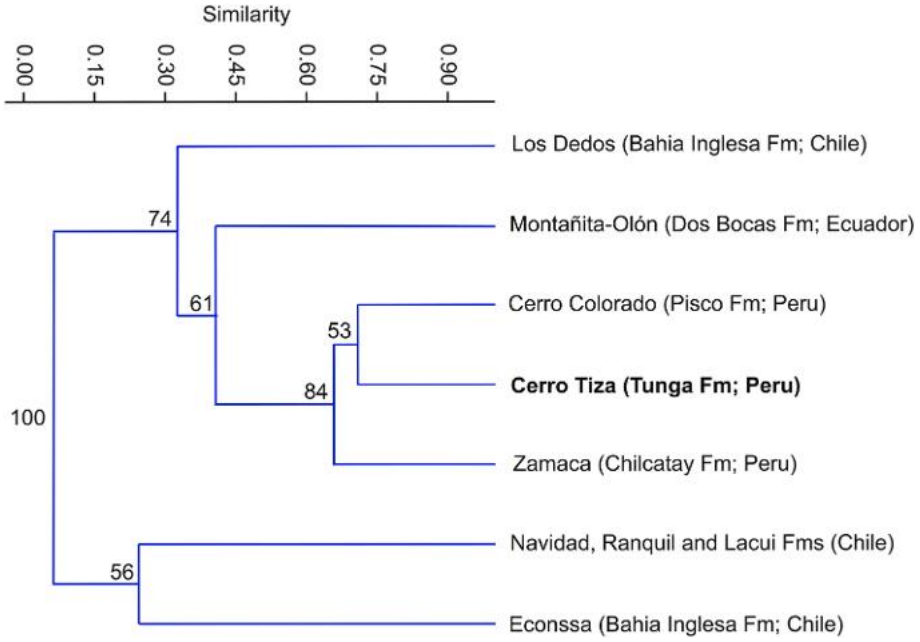

Fig. 10. Cluster analysis based on the Dice index showing the Miocene South American elasmobranch assemblages hierarchically grouped together as to reflect their palaeoecological and palaeoenvironmental similarity. Numbers on each node are bootstrap values (1000 replicates).

smaller shark and stingray species as well as to their likely prey.

5.2. Paleodiversity, paleoecological and paleoenvironmental significance

The Early Miocene elasmobranch assemblage of the Tunga Formation at Cerro Tiza comprises seven extinct species out of at least 17, but only three genera are extinct (Table 1). Although the Cerro Tiza assemblage exhibits a similar number of species and genera compared to the other Peruvian assemblages from Cerro Colorado (Pisco Formation) and Zamaca (Chilcatay Formation), the three localities are characterized by a different taxonomic composition. Eight species [the lamniforms *Anotodus retroflexus*, *Isurus oxyrinchus* and *Cosmopolitodus hastalis*, and the carcharhiniforms *Carcharhinus brachyurus*, *C. leucas* (or *C.* cf. *leucas*), *Galeocerdo aduncus* (or *G.* cf. *aduncus*), *Negaprion brevirostris* (or *N.* cf. *brevirostris*), and *Physogaleus contortus*] are present in all the three Peruvian assemblages (Table 2). Conversely, the megatooth shark *Otodus chubutensis* and the threshers *Alopias supercilious* and *A. vulpinus* (or cf. *vulpinus*) are only present at Cerro Tiza and Zamaca, whereas *Carcharias taurus*, *Pseudocarcharias* and *Aetobatus* occur in both the Cerro Tiza and Cerro Colorado assemblages. In terms of abundance, *Isurus* and *Cosmopolitodus* are by far the most abundant taxa at Cerro Tiza (40.5 and 35.7%, respectively), whereas *Carcharhinus* and *Cosmopolitodus* are the

most represented at the Zamaca site (33.7 and 28.7%, respectively), and *Carcharhinus* is by far the dominant genus at Cerro Colorado (81.8%), with *C. brachyurus* alone representing more than 95.5% of the *Carcharhinus* teeth (Table 2). Taken together, these data indicate that the Cerro Tiza assemblage allows for documenting the composition of an Aquitanian elasmobranch fauna from the East Pisco Basin – one that can be placed within a regional South American comparative framework.

Although the paleoenvironmental interpretation of the Early Miocene elasmobranch assemblage of Cerro Tiza (Fig. 9; Table 1) might point to an epipelagic, outer shelf to upper bathyal signal, if the ecology of the most abundant taxa (*Isurus* and *Cosmopolitodus*) is taken into account, this inference should be treated cautiously in light of the wave-ravinement surface and transgressive condensed-lag nature of the tooth-rich phosphorite bed, as well as of the potential for time-averaging and mechanical size selection that would have occurred during reworking (see Taphonomic remarks above). Conversely, if the paleoecology of all taxa is considered, independently from their abundances, their bathymetric preferences and habitats are broadly consistent with the transgressive nature of the deposit as revealed by sedimentological observations, suggesting as they do a shelf (shoreline to shelf break) setting.

Even acknowledging the taphonomic bias discussed above, the abundant occurrence of medium-to large-sized predatory sharks suggests that upper-level predators formed a conspicuous component of the source fauna. However, because phosphoritic condensation likely enhanced the representation of robust teeth, this pattern should not be read as a direct census of the original community structure. For example, *Cosmopolitodus hastalis* was a cosmopolite inhabitant of the Miocene–-Pliocene oceans worldwide. Fossil evidence indicates that it also occupied high trophic positions. Trace fossil studies have documented bite marks attributed to *C. hastalis* on bones of marine mammals (e.g., dolphins), providing direct evidence of interactions with large vertebrate preys in the fossil record (Godfrey et al., 2025), as also corroborated by isotope analyses (Kast et al., 2022; McCormack et al., 2022). On the other hand, exceptional fossil specimens of *C. hastalis* with preserved stomach contents, including remains of schooling clupeids such as pilchards (*Sardinops*), demonstrate that fishes were a significant component of the diet of *C. hastalis*, at least in juvenile individuals, and imply that it exploited abundant fish resources in productive Miocene coastal environments (Collareta et al., 2017). The same can be said for the megatooth otodontid *Otodus chubutensis* that likely occupied the highest trophic level within the Cerro Tiza assemblage (Table 1; see also Carrillo-Briceño et al., 2019; Landini et al., 2019).

The presence of these taxa in the Tunga Formation assemblage is consistent with an ecological structure where medium-to large-sized predatory sharks played a central role in energy transfer through the marine food web. *Isurus oxyrinchus* likely occupied a trophic niche focused on actively predating abundant nektonic fishes, while *C. hastalis* indicates the presence of predators capable of both large-prey interactions (including marine vertebrates) and substantial piscivory. Taken with caution, this pattern is consistent with an ecologically rich trophic network, including multiple high-level predators exploiting diverse nektonic prey resources.

Taxonomic comparisons between the Cerro Tiza elasmobranch assemblage and other Miocene South American faunas (Table 2) provide a more complete perspective about the diversity of the Cerro Tiza fauna that allows for the following considerations: 1) The Cerro Tiza assemblage, along with those from other Peruvian sites as well as from Navidad and Econssa (Chile), is one of the less diverse Miocene elasmobranch assemblages. Even if the sample abundances at the three Peruvian sites is different (from 533 specimens at Cerro Tiza to 3918 specimens at Zamaca), results from the Good's u value indicate that differences in taxonomic composition and diversity might not be the result of collection or taphonomic bias; 2) the majority of elasmobranch taxa from Cerro Tiza consist of 4th level predators, with a predominantly piscivorous diet, although their juveniles certainly occupied lower trophic levels, whereas adult lamnid individuals were likely capable of preying upon marine mammals (e.g., Bianucci et al., 2010; Ehret et al., 2012).

The presence and abundance of epipelagic, piscivorous and eurytrophic sharks is consistent with the sedimentological and paleoenvironmental setting of another phosphorite deposit described by Bosio et al. (2024) in Middle Miocene strata of the Pisco Formation close to Cerro Submarino, in the East Pisco Basin. According to their results, the Miocene phosphorites of the Pisco Formation formed just below the sediment-water interface during early transgression, in shallow-marine conditions with high biological productivity, low net sedimentation rates, and suboxic conditions at and beneath the seafloor. Bosio et al. (2024) also noted that phosphorites in the Ica Desert mantle all major stratigraphic unconformities throughout the Miocene at least. This implies that the same basic mechanism (transgressive ravinement and condensation under upwelling) was likely operating already during deposition of the underlying Chilcatay and Tunga Formations. It is therefore reasonable, within the limits of the available data, to treat the Chilcatay and Tunga phosphorite lags as the older expression of the same ravinement system described by Bosio et al. (2024). The authors also linked the Pisco phosphogenesis to the intense coastal upwelling along the Peru-Chile margin, resulting in very high primary productivity and a large flux of organic matter (and phosphorus) to the seafloor. This supported a vertebrate trophic web where small-sized, epipelagic and schooling fishes such as *Sardinops humboldti* (see Carnevale et al., 2026) represented a fundamental prey for higher-trophic level fishes and marine mammals (Collareta et al., 2015, 2017, 2021b).

For the Chilcatay Formation, independent works on the vertebrate assemblages at Ullujaya and Zamaca depict paleobiotopes formed by shallow-marine, semi-enclosed to sheltered embayment settings, connected to both riverine and open-ocean waters, and vertebrate communities dominated by toothed cetaceans plus a diverse elasmobranch fauna, with *Cosmopolitodus hastalis* and other large sharks being particularly abundant, often as juveniles, in nearshore settings (Bianucci et al., 2018; Landini et al., 2019).

In this perspective, upwelling and highly productive conditions that drove phosphogenesis in the Late Miocene depositional setting of the Pisco Formation almost certainly already existed in the Early Miocene (same margin, same upwelling system, same basin architecture). Those conditions would have favoured huge schools of small- and medium-sized teleosts, which were preyed upon by a variety of sharks, with the large sharks *Isurus*, *Cosmopolitodus* and *Otodus* being also capable to prey upon large mammals.

6. Conclusions

The Cerro Tiza phosphorite lag documents the earliest Neogene elasmobranch assemblage from the East Pisco Basin of Peru. Crucially, this fossil vertebrate fauna is one of the few of Aquitanian age to be currently known the Pacific margin of South America. The assemblage includes at least 17 species and 15 genera, and is numerically dominated by lamniform sharks, especially *Cosmopolitodus hastalis* and *Isurus oxyrinchus*. Sedimentological and taphonomic evidence indicates that this dominance was likely amplified by condensation, reworking and preferential preservation within a transgressive phosphorite lag. Paleoecological and paleoenvironmental implications are broadly compatible with a shelf setting and a predator-rich assemblage, although they should be treated cautiously in the light of the sedimentological and taphonomic signature of the embedding deposit.

CRediT authorship contribution statement

Giuseppe Marramà: Conceptualization, Data curation, Formal analysis, Funding acquisition, Investigation, Methodology, Software, Supervision, Validation, Visualization, Writing – original draft. **Alberto Collareta:** Conceptualization, Data curation, Funding acquisition,

Project administration, Validation, Writing – review & editing. **Giulia Bosio:** Data curation, Formal analysis, Methodology, Software, Visualization, Writing – review & editing. **Giovanni Bianucci:** Data curation, Funding acquisition, Writing – review & editing. **Elisa Malinverno:** Data curation, Formal analysis, Funding acquisition, Methodology, Validation, Writing – review & editing. **Claudio Di Celma:** Data curation, Funding acquisition, Validation, Writing – review & editing. **Francesco Nobile:** Writing – review & editing. **Luca Pellegrino:** Data curation, Writing – review & editing. **Alí Altamirano-Sierra:** Writing – review & editing. **Mario Urbina:** Writing – review & editing. **Igor M. Villa:** Data curation, Formal analysis, Writing – review & editing. **Jaime A. Villafaña:** Data curation, Writing – review & editing. **Alice Zanda:** Formal analysis, Writing – review & editing. **Giorgio Carnevale:** Conceptualization, Data curation, Funding acquisition, Investigation, Writing – review & editing.

Declaration of competing interest

The authors declare that they have no known competing financial interests or personal relationships that could have appeared to influence the work reported in this paper.

Acknowledgments

The authors wish to thank Rafael Varas-Malca, Walter Aguirre, Rodolfo Salas-Gismondi, César Chacaltana-Budiel and Luz Tejada-Medina for the support in the field and in the laboratories. We especially thank to Nicoletta Fusi and Valentina Barberini for helping with grain-size and dating analyses. Compositional analyses were performed at the EPMA facility of the Unitech COSPECT at the University of Milan (Italy) with the assistance of Andrea Risplendente. The manuscript was greatly improved with the constructive suggestions provided by two anonymous reviewers and by editorial comments by Francisco J. Vega. We acknowledge financial support by the European Union – NextGenerationEU, Mission 4, Component 2, CUP I53D23002070 006, Project Title: BIOVERTICES (BIOdiversity of VERTebrates In the CEnozoic Sea), and by the Fondo Nacional de Desarrollo Cientıfico y Tecnologico [-ANID/FONDECYT 3230610].

Appendix A. Supplementary data

Supplementary data to this article can be found online at https://doi.org/10.1016/j.jsames.2026.106080.

Data availability

Data will be made available on request.

References

Agassiz, L., 1834. Recherches sur les poissons fossiles - Tome II. Imprimerie de Petitpierre, Neuchâtel.

Aguilera, O., Luz, Z., Carrillo-Briceño, J.D., Kocsis, L., Vennemann, T.W., De Toledo, P. M., Nogueira, A., Amorim, K.B., Moraes-Santos, H., Polck, M.R., Ruivo, M. de L., Linhares, A.P., Monteiro-Neto, C., 2017. Neogene sharks and rays from the Brazilian 'Blue Amazon'. PLoS One 12 (8), e0182740.

Akiba, F., Hiramatsu, C., Yanagisawa, Y., 1993. A Cenozoic diatom genus *Cavitauts* Williams; an emended description and two new biostratigraphically useful species, *C. lanceolatus* and *C. rectus* from Japan. Bulletin of the National Science Museum, Tokyo, Series C: Geology and Paleontology 19 (1), 11–39.

Alroy, J., 2010. Geographical, environmental and intrinsic biotic controls on Phanerozoic marine diversification. Palaeontology 53, 1211–1235. https://doi.org/10.1111/j.1475-4983.2010.01011.x.

Ameghino, F., 1901. L'âge des formations sédimentaires de Patagonie. An. Soc. Cient. Argent. 51, 65–91.

Antonijevic, S.K., Wagner, L.S., Kumar, A., Beck, S.L., Long, M.D., Zandt, G., Tavera, H., Condori, C., 2015. The role of ridges in the formation and longevity of flat slabs. Nature 524, 212–215. https://doi.org/10.1038/nature14648.

Ayala-Carazas, L., Viveen, W., Baby, P., Uribe-Ventura, R., Binnie, S.A., Sanjurjo-Sánchez, J., Beltrán-Castañon, C., 2026. Quaternary tectonic shortening and uplift of the Peruvian forearc due to subduction of the Nazca Ridge. Gondwana Res. 153, 323–343. https://doi.org/10.1016/j.gr.2025.12.008.

Barron, J.A., DeVries, T.J., Coenen, J.J., 2026. Miocene evolution of the Humboldt Current. Palaeogeogr. Palaeoclimatol. Palaeoecol. 686, 113558. https://doi.org/10.1016/j.palaeo.2026.113558.

Benton, M.J., Dunhill, A.M., Lloyd, G.T., Marx, F.G., 2011. Assessing the quality of the fossil record: insights from vertebrates. Geol. Soc. Spec. Publ. 358, 63–94. https://doi.org/10.1144/SP358.

Bianucci, G., Collareta, A., Bosio, G., Landini, W., Gariboldi, K., Gioncada, A., Lambert, O., Malinverno, E., de Muizon, C., Varas-Malca, R., Villa, I.M., Coletti, G., Urbina, M., Di Celma, C., 2018. Taphonomy and palaeoecology of the lower Miocene marine vertebrate assemblage of Ullujaya (Chilcatay Formation, East Pisco Basin, southern Peru). Palaeogeogr. Palaeoclimatol. Palaeoecol. 511, 256–279. https://doi.org/10.1016/j.palaeo.2018.08.013.

Bianucci, G., Sorce, B., Storai, T., Landini, W., 2010. Killing in the Pliocene: shark attack on a dolphin from Italy. Palaeontology 53, 457–470. https://doi.org/10.1111/j.1475-4983.2010.00945.x.

Bishop, B.T., Beck, S.L., Zandt, G., Wagner, L., Long, M., Antonijevic, S.K., Kumar, A., Tavera, H., 2017. Causes and consequences of flat-slab subduction in southern Peru. Geosphere 13, 1392–1407. https://doi.org/10.1130/GES01440.1.

Blott, S.J., Pye, K., 2001. GRADISTAT: a grain size distribution and statistics package for the analysis of unconsolidated sediments. Earth Surf. Process. Landf. 26 (11), 1237–1248.

Bosio, G., Bianucci, G., Collareta, A., Landini, W., Urbina, M., Di Celma, C., 2022. Ultrastructure, composition, and 87Sr/86Sr dating of shark teeth from lower Miocene sediments of southern Peru. J. South Am. Earth Sci. 118, 103909. https://doi.org/10.1016/j.jsames.2022.103909.

Bosio, G., Gioncada, A., Malinverno, E., Coletti, G., Collareta, A., Mariani, L., Cavallo, A., Bianucci, G., Urbina, M., Di, C., 2024. Unraveling marine phosphogenesis along the Miocene coast of Peru : origin and sedimentological significance of the Pisco Formation phosphorites. Mar. Petrol. Geol. 167, 106941. https://doi.org/10.1016/j.marpetgeo.2024.106941.

Bosio, G., Gioncada, A., Malinverno, E., Di Celma, C., Villa, I.M., Cataldi, G., Gariboldi, K., Collareta, A., Urbina, M., Bianucci, G., 2019. Chemical and petrographic fingerprinting of volcanic ashes as a tool for high-resolution stratigraphy of the upper Miocene Pisco Formation (Peru). J. Geol. Soc. 176, 13–28.

Bosio, G., Malinverno, E., Villa, I.M., Di Celma, C., Gariboldi, K., Gioncada, A., Barberini, V., Urbina, M., Bianucci, G., 2020. Tephrochronology and chronostratigraphy of the Miocene Chilcatay and Pisco formations (East Pisco basin, Peru). Newsl. Stratigr. 53 (2), 213–247.

Bown, P.R., Young, J.R., 1998. Introduction. In: Bown, P.R. (Ed.), Calcareous Nannofossil Biostratigraphy, British Micropalaeontology Society Series. Chapman & Hall, London, pp. 1–15.

Bukry, D., 1981. Synthesis of Silicoflagellate Stratigraphy for Maastrichtian to Quaternary Marine Sediments, vol. 32. SEPM Spec. Publ., pp. 433–444

Cappetta, H., 1987. Handbook of Paleoichthyology. In: Chondrichthyes II, 3B. Gustav Fischer Verlag, Stuttgart.

Cappetta, H., 2012. Handbook of Paleoichthyology – Chondrichthyes – Mesozoic and Cenozoic Elasmobranchii: Teeth. Verlag Dr. Friedrich Pfeil, Munich.

Carnevale, G., Pellegrino, L., Bosio, G., Bianucci, G., Collareta, C., Di Celma, C. Di, Malinverno, E., Ramirez Ampuero, A.A., Tejada-Medina, L., Chacaltana, C., Urbina, M., Marramà, G., 2026. Fossil sardines from the Pisco Formation (Miocene), Peru: taxonomy, taphonomy, and paleoecology. Palaeoworld 35, 201049. https://doi.org/10.1016/j.palwor.2025.201049.

Carrillo-Briceño, J.D., Aguilera, O., De Gracia, C., Aguirre-Fernandez, G., Kindlimann, R., Sánchez-Villagra, M., 2016a. An Early Neogene Elasmobranch fauna from the southern Caribbean (Western Venezuela). Palaeontol. Electron. 19 (2). https://doi.org/10.26879/664.

Carrillo-Briceño, J.D., Aguilera, O.A., Rodriguez, F., 2014. Fossil chondrichthyes from the central eastern Pacific Ocean and their paleoceanographic significance. J. South Am. Earth Sci. 51, 76–90.

Carrillo-Briceño, J.D., Argyriou, T., Zapata, V., Kindlimann, R., Jaramillo, C., 2016b. A new early Miocene (Aquitanian) Elasmobranchii assemblage from the La Guajira Peninsula, Colombia. Ameghiniana 53, 77–99.

Carrillo-Briceño, J.D., De Gracia, C., Pimiento, C., Aguilera, O.A., Kindlimann, R., Santamarina, P., Jaramillo, C., 2015a. A new Late Miocene chondrichthyan assemblage from the Chagres Formation, Panama. J. South Am. Earth Sci. 60, 56–70. https://doi.org/10.1016/j.jsames.2015.02.001.

Carrillo-Briceño, J.D., Gonzales-Barba, G., Landaeta, M.F., Nielsen, S.N., 2013. Condrictios fosiles del Plioceno Superior de la Formacion Horcon, Region de Valparaíso, Chile Central. Rev. Chil. Hist. Nat. 86, 191–206.

Carrillo-Briceño, J.D., Luz, Z., Hendy, A., Kocsis, L., Aguilera, O., Vennemann, T., 2019. Neogene Caribbean elasmobranchs: diversity, paleoecology and paleoenvironmental significance of the Cocinetas Basin assemblage (Guajira Peninsula, Colombia). Biogeosciences 16, 33–56. https://doi.org/10.5194/bg-16-33-2019.

Carrillo-Briceño, J.D., Maxwell, E., Aguilera, O.A., Sánchez, R., Sánchez-Villagra, M.R., 2015b. Sawfishes and other elasmobranch assemblages from the Mio-Pliocene of the South Caribbean (Urumaco Sequence, Northwestern Venezuela). PLoS One 10 (10), e0139230. https://doi.org/10.1371/journal.pone.0139230.

Carrillo-Briceño, J.D., Villafaña, J.A., de Gracia, C., Flores-Alcívar, F.F., Kindlimann, R., Abella, J., Fernando Flores-Alcívar, F., Kindlimann, R., Abella, J., 2020. Diversity and paleoenvironmental implications of an elasmobranch assemblage from the Oligocene-Miocene boundary of Ecuador. PeerJ 1–27. https://doi.org/10.7717/peerj.9051, 2020.

Chandler, R.E., Chiswell, K.E., Faulkner, G.D., 2006. Quantifying a possible Miocene phyletic change in *Hemipristis* (Chondrichthyes) teeth. Palaeontol. Electron. 9, 4A: 14p. http://palaeo-electronica.org/paleo/2006_1/teeth/issue1_06.htm.

Chao, A., Jost, L., 2012. Coverage-based rarefaction and extrapolation: standardizing samples by completeness rather than size. Ecology 93, 2533–2547.

Chávez-Hoffmeister, M.F., Villafaña, J.A., 2023. The Neogene record of cartilaginous fishes (Chondrichthyes: Holocephali , Elasmobranchii) from northern Chile : a review and identification guide. J. South Am. Earth Sci. 124, 104230. https://doi.org/10.1016/j.jsames.2023.104230.

Ciattoni, S., Cella, F., Mazzoli, S., Zambrano, M., Megna, A., Santini, S., Butler, R., Pierantoni, P.P., Di Celma, C., 2025. Lithosphere architecture along the axis of the subducting aseismic Nazca Ridge (Peruvian Active Margin). Tectonics 44. https://doi.org/10.1029/2024TC008514 e2024TC008514.

Cigala-Fulgosi, F., Casati, S., Orlandini, A., Persico, D., 2009. A Small Fossil Fish Fauna, Rich in *Chlamydoselachus* Teeth, from the Late Pliocene of Tuscany (Siena, Central Italy), vol. 6. Cainozoic research, pp. 3–23.

Coenen, J.J., Barron, J.A., DeVries, T.J., 2025. Uppermost Oligocene and Miocene diatom biostratigraphy of Ocean Drilling Program Sites 682 and 688 from the Peru Margin. Stratigraphy 22 (3), 155–180.

Collareta, A., Di Celma, C., Bosio, G., Pierantoni, P.P., Malinverno, E., Lambert, O., Marx, F.G., Landini, W., Urbina, M., Bianucci, G., 2021a. Distribution and paleoenvironmental framework of middle Miocene marine vertebrates along the western side of the lower Ica Valley (East Pisco Basin, Peru). J. Maps 17 (2), 7–17.

Collareta, A., Lambert, O., Marx, F.G., Muizon, C. De, Varas-Malca, R., Landini, W., Bosio, G., Malinverno, E., Gariboldi, K., Gioncada, A., Urbina, M., Bianucci, G., 2021b. Vertebrate Palaeoecology of the Pisco Formation (Miocene , Peru): glimpses into the Ancient Humboldt Current Ecosystem. J. Mar. Sci. Eng. 9 (11), 1188. https://doi.org/10.3390/jmse9111188.

Collareta, A., Landini, W., Chacaltana, C., Valdivia, W., Altamirano-Sierra, A., Urbina-Schmitt, M., Bianucci, G., 2017. A well preserved skeleton of the fossil shark *Cosmopolitodus hastalis* from the late Miocene of Peru , featuring fish remains as fossilized stomach contents. Riv. Ital. Paleontol. Stratigr. 123, 11–22. https://doi.org/10.13130/2039-4942/8005.

Collareta, A., Landini, W., Lambert, O., Post, K., Tinelli, C., Di Celma, C., Panetta, D., Tripodi, M., Salvadori, P.A., Caramella, D., Marchi, D., Urbina, M., Bianucci, G., 2015. Piscivory in a Miocene Cetotheriidae of Peru : first record of fossilized stomach content for an extinct baleen-bearing whale. Sci. Nat. 102, 70. https://doi.org/10.1007/s00114-015-1319-y.

Compagno, L.J.V., 1973. Interrelationships of living elasmobranchs. In: Greenwood, P., Miles, R., Patterson, C. (Eds.), Interrelationships of Fishes. Academic Press, New York, pp. 15–61.

Contreras-Reyes, E., Muñoz-Linford, P., Cortés-Rivas, V., Bello-González, J.P., Ruiz, J.A., Krabbenhoeft, A., 2019. Structure of the collision zone between the Nazca Ridge and the Peruvian convergent margin: geodynamic and seismotectonic implications. Tectonics 38, 3416–3435. https://doi.org/10.1029/2019TC005637.

Cortés, E., 1999. Standardized diet compositions and trophic levels of sharks. ICES (Int. Counc. Explor. Sea) J. Mar. Sci. 56, 707–717. https://doi.org/10.1006/jmsc.1999.0489.

Decou, A., von Eynatten, H., Mamani, M., Sempéré, T., Worner, G., 2011. Cenozoic forearc basin sediments in Southern Peru (15-18 degrees S): stratigraphic and heavy mineral constraints for Eocene to Miocene evolution of the Central Andes. Sedimentary Geology 237, 55–72.

DeVries, J.T., 1998. Oligocene deposition and Cenozoic sequence boundaries in the Pisco Basin (Peru). J. South Am. Earth Sci. 11, 217–231. https://doi.org/10.1016/S0895-9811(98)00014-5.

DeVries, J.T., 2017. Eocene stratigraphy and depositional history near Puerto Caballas (East Pisco Basin, Peru). Bol. Soc. Geol. Peru 112, 39–52.

DeVries, J.T., Barron, J.A., Ochoa, D., McDougalle, K., 2024. Chronology and Paleoenvironment of the Tunga Formation, a new lowermost Miocene sequence in the East Pisco Basin of southern Peru. Stratigraphy 21, 190–225.

DeVries, J.T., Urbina, M., Jud, N.A., 2017. The Eocene-Oligocene Otuma depositional sequence (East Pisco Basin, Peru): paleogeographic and paleoceanographic implications of new data. Bol. Soc. Geol. Peru 112, 14–38.

DeVries, J.T., Jud, N.A., 2017. Lithofacies patterns and paleogeography of the Miocene Chilcatay and lower Pisco depositional sequences (East Pisco Basin, Peru). Bol. Soc. Geol. Peru 8, 124–167.

Di Celma, C., Malinverno, E., Bosio, G., Collareta, A., Gariboldi, K., Gioncada, A., Molli, G., Basso, D., Malca, V., Varas-Malca, R.M., Pierantoni, P.P., Villa, I.M., Lambert, O., Landini, W., Sarti, G., Cantalamessa, G., Urbina, M., Bianucci, G., 2017. Sequence stratigraphy and paleontology of the Upper Miocene Pisco Formation along the western side of the lower Ica Valley (Ica Desert, Peru). Riv. Ital. Paleontol. Stratigr. 123, 255–273. https://doi.org/10.13130/2039-4942/8373.

Di Celma, C., Malinverno, E., Bosio, G., Gariboldi, K., Collareta, A., Gioncada, A., Landini, W., Pierantoni, P.P., Bianucci, G., 2018. Intraformational unconformities as a record of late Miocene eustatic falls of sea level in the Pisco Formation (southern Peru). J. Maps 14, 607–619. https://doi.org/10.1080/17445647.2018.1517701.

Di Celma, C., Pierantoni, P.P., Volatili, T., Molli, G., Mazzoli, S., Sarti, G., Ciattoni, S., Bosio, G., Malinverno, E., Collareta, A., Gariboldi, K., Gioncada, A., Jablonska, D., Landini, W., Urbina, M., Bianucci, G., 2022. Towards deciphering the Cenozoic evolution of the East Pisco Basin (southern Peru). J. Maps 18 (2), 397–412. https://doi.org/10.1080/17445647.2022.2072780.

Dice, L.R., 1945. Measures of the amount of ecologic association between species. Ecology 26, 297–302.

Dunbar, R.B., Marty, R.C., Baker, P.A., 1990. Cenozoic marine sedimentation in the Sechura and Pisco basins, Peru. Palaeogeogr. Palaeoclimatol. Palaeoecol. 77, 235–261. https://doi.org/10.1016/0031-0182(90)90179-B.

Ebersole, J.A., Cicimurri, D.J., Stringer, G.L., 2019. Taxonomy and biostratigraphy of the elasmobranchs and bony fishes (Chondrichthyes and Osteichthyes) of the lower-to-middle Eocene (Ypresian to Bartonian) Claiborne Group in Alabama, USA, including an analysis of otoliths. European Journal of Taxonomy 585, 1–274. https://doi.org/10.5852/ejt.2019.585.

Ebersole, J.A., Ebersole, S.M., Cicimurri, D.J., 2017. The occurrence of early Pleistocene marine fish remains from the Gulf Coast of Mobile County, Alabama, USA. Palaeodiversity 10, 97–115. https://doi.org/10.18476/pale.v10.a6.

Ehret, D.J., Macfadden, B.J., Jones, D.S., Devries, T.J., Foster, D.A., Salas-Gismondi, R., Vries, T.J.D.E., Foster, D.A., Salas-Gismondi, R., 2012. Origin of the white shark *Carcharodon* (Lamniformes: Lamnidae) based on recalibration of the Upper Neogene Pisco Formation of Peru. Palaeontology 55, 1139–1153. https://doi.org/10.1111/j.1475-4983.2012.01201.x.

Esperante, R., Brand, L., Nick, K., Poma, O., Urbina, M., 2008. Exceptional occurrence of fossil baleen in shallow marine sediments of the Neogene Pisco Formation, Southern Peru. Palaeogeogr. Palaeoclimatol. Palaeoecol. 257, 344–360.

Föllmi, K.B., Garrison, R.E., Grimm, K.A., 1991. Stratification in phosphatic sediments: illustrations from the Neogene of Central California. Cycles and Events in Stratigraphy 1991, 492–507.

Froese, R., Pauly, D., 2025. FishBase. World wide web electronic publication. https://www.fishbase.org. (Accessed 20 October 2025).

Gastaldello, M.E., Bosio, G., Di Celma, C., Bianucci, G., Collareta, A., Mazzoli, S., Pellegrino, L., Villa, I. M., Urbina, M., Malinverno, E. (in press). The stratigraphic record of the Eocene–Oligocene transition in the East Pisco Basin (Peru): a phytoplankton perspective. Newsl. Stratigr.

Glikman, L.S., 1964. Sharks of the Paleogene and their Stratigraphic Significance. Nauka Press, Moscow [in Russian].

Godfrey, S.J., Perez, V.J., Jones, M., Chapman, P.F., Spencer, N., Osborne, J.E., New, J. E., 2025. New light on the trophic ecology of *Carcharodon hastalis* from teeth embedded in Miocene cetacean vertebrae from Calvert Cliffs in Maryland , USA. Acta Palaeontol. Pol. 70, 329–337.

Gotelli, N.J., Colwell, R.K., 2001. Quantifying biodiversity: procedures and pitfalls in the measurement and comparison of species richness. Ecol. Lett. 4, 379–391.

Griggs, A.J., Davies, S.M., Abbott, P.M., Rasmussen, T.L., Palmer, A.P., 2014. Optimising the use of marine tephrochronology in the North Atlantic: a detailed investigation of the Faroe Marine Ash Zones II, III and IV. Quat. Sci. Rev. 106, 122–139.

Gutscher, M.A., Spakman, W., Bijwaard, H., Engdahl, E.R., 2000. Geodynamics of flat subduction: seismicity and tomographic constraints from the Andean margin. Tectonics 19 (5), 814–833. https://doi.org/10.1029/1999TC001152.

Hammer, Ø., Harper, D.A.T., Ryan, P., 2001. PAST: Paleontological Statistics software package for education and data analysis. Palaeontol. Electron. 4, 1–9.

Hampel, A., 2002. The migration history of the Nazca Ridge along the Peruvian active margin: a re-evaluation. Earth Planet Sci. Lett. 203 (2), 665–679. https://doi.org/10.1016/S0012-821X(02)00859-2.

Herman, J., 1979. Réflexions sur la systématique des Galeoidei et sur les affinités du genre *Cetorhinus* à l'occasion de la découverte d'éléments de la denture d'un exemplaire fossile dans les Sables du Kattendijk à Kallo (Pliocène inférieur, Belgique). Ann. Soc. Geol. Belg. 102, 357–377.

Höltke, O., Maxwell, E.E., Pollerspöck, J., Rasser, M.W., 2022. The shark and ray fauna of the Upper Marine Molasse (Lower Miocene) of Rengetsweiler (Baden-Württemberg, SW Germany). Neues Jahrbuch fur Geologie und Palaontologie - Abhandlungen 303, 89–122. https://doi.org/10.1127/njgpa/2022/1038.

Höltke, O., Maxwell, E.E., Rasser, M.W., 2024. A Review of the paleobiology of some Neogene sharks and the fossil records of extant shark species. Diversity 16 (3), 147. https://doi.org/10.3390/d16030147.

Hovestadt, D.C., Hovestadt-Euler, M., 2013. Generic assessment and reallocation of Cenozoic myliobatins based on new information of tooth, tooth plate and caudal spine morphology of extant taxa. PALAEONTOS 24, 1–66.

Hsu, J.T., 1992. Quaternary uplift of the Peruvian coast related to the subduction of the Nazca Ridge: 13.5 to 15.6° south latitude. Quat. Int. 15/16, 87–97. https://doi.org/10.1016/1040-6182(92)90038-4.

Jost, L., Chao, A., Chazdon, R.L., 2011. Compositional similarity and β (beta) diversity. In: Magurran, A.E., McGill, B.J. (Eds.), Biological diversity: frontiers in measurement and assessment. Oxford Universi011ty Press, Oxford, pp. 66–84.

Kast, E.R., Griffiths, M.L., Kim, S.L., Rao, Z.C., Shimada, K., Becker, M.A., Maisch, H.M., Eagle, R.A., Clarke, C.A., Neumann, A.N., Karnes, M.E., Lüdecke, T., Leichliter, J.N., Martínez-García, A., 2022. Cenozoic megatooth sharks occupied extremely high trophic positions. Sci. Adv. 8 eabl6529.

Kent, B.W., 2018. The cartilaginous fishes (chimaeras, sharks and rays) of Calvert Cliffs, Maryland, USA. In: Kent, B.W. (Ed.), Geology and Vertebrate Paleontology of Calvert Cliffs. Smithsonian Institution Press, Washington.

Kidwell, S.M., 1989. Stratigraphic condensation of marine transgressive records: origin of major shell deposits in the Miocene of Maryland. J. Geol. 97, 1–24. https://doi.org/10.1086/629278.

Kulm, L.D., Resig, J.M., Thornburg, T.M., Schrader, H.J., 1982. Cenozoic structure, stratigraphy and tectonics of the central Peru forearc. In: Legget, J.K. (Ed.), Trench and forearc geology: Sedimentation and tectonics on modern and ancient plate margins. Blackwells, pp. 151–169.

Landini, W., Altamirano-Sierra, A., Collareta, A., Di Celma, C., Urbina, M., Bianucci, G., 2017a. The late Miocene elasmobranch assemblage from Cerro Colorado (Pisco Formation, Peru). J. South Am. Earth Sci. 73, 168–190. https://doi.org/10.1016/j.jsames.2016.12.010.

Landini, W., Collareta, A., Di, C., Malinverno, E., Urbina, M., Bianucci, G., 2019. The early Miocene elasmobranch assemblage from Zamaca (Chilcatay Formation, Peru). J. South Am. Earth Sci. 91, 352–371. https://doi.org/10.1016/j.jsames.2018.08.004.

Landini, W., Collareta, A., Pesci, F., Di, C., Urbina, M., Bianucci, G., 2017b. A secondary nursery area for the copper shark *Carcharhinus brachyurus* from the late Miocene of Peru. J. South Am. Earth Sci. 78, 164–174. https://doi.org/10.1016/j.jsames.2017.07.003.

Laurito, C.A., Calvo, C., Valerio, A.L., Calvo, A., Chacón, R., 2014. Ictiofauna del Mioceno Inferior de la localidad de Pacuare de Tres Equis, Formación Río Banano, provincia de Cartago, Costa Rica, y descripción de un nuevo género y una nueva especie de Scaridae. Rev. Geol. Am. Cent. 153–192. https://doi.org/10.15517/rgac.v0i50.15121.

Lazarus, D., Barron, J., Renaudie, J., Diver, P., Türke, A., 2014. Cenozoic planktonic marine diatom diversity and correlation to climate change. PLoS One 9 (1), e84857.

Long, D.J., 1993. Late Miocene and Early Pliocene fish assemblages from the north central coast of Chile. Tert. Res. 14, 117–126.

Lowe, D.J., 2011. Tephrochronology and its application: a review. Quat. Geochronol. 6 (2), 107–153.

Ludwig, K.R., 2012. User's Manual for Isoplot Version 3.75–4.15: a Geochronological Toolkit for Microsoft Excel. Berkeley Geochronological Center Special Publication, California, p. 76.

Macharé, J., Ortlieb, L., 1992. Plio-Quaternary vertical motions and the subduction of the Nazca Ridge, central coast of Peru. Tectonophysics 205, 97–108. https://doi.org/10.1016/0040-1951(92)90420-B.

Magurran, A.E., 2004. Measuring Biological Diversity. Blackwell Publishing, Oxford.

Maisch, H.M., Becker, M.A., Perez, V.J., Shimada, K., 2025. Sharks and rays (Chondrichthyes: Elasmobranchii) from the Peace River and Tamiami formations (Late Miocene – early Pliocene) on the submerged continental shelf near Venice, Florida, USA. Palaeontol. Electron. 28, a49.

Malyshkina, T.P., Nazarkin, M.V., Solovyow, A.V., 2024. An oldest record of the shark *Cosmopolitodus planus* (Lamnidae) from the Lower Miocene of the Sakhalin, Russia. J. Ichthyol. 64, 72–79. https://doi.org/10.1134/S0032945224010144.

Marramà, G., Bannikov, A.F., Tyler, J.C., Zorzin, R., Carnevale, G., 2016. Controlled excavations in the Pesciara and Monte Postale sites provide new insights about the palaeoecology and taphonomy of the fish assemblages of the Eocene Bolca Konservat-Lagerstätte, Italy. Palaeogeogr. Palaeoclimatol. Palaeoecol. 454, 228–245. https://doi.org/10.1016/j.palaeo.2016.04.021.

Marramà, G., Carnevale, G., Kriwet, J., 2021. Diversity, palaeoecology and palaeoenvironmental significance of the Eocene chondrichthyan assemblages of the Bolca Lagerstätte, Italy. Lethaia 54 (5), 736–751. https://doi.org/10.1111/let.12436.

Martinez, P.R., Carrapa, B., Clementz, M.T., Gutstein, C.S., Worrell, W.E., Hasiotis, S.T., Martínez-López, J.G., Munoz, F.A., 2025. Controls on late Miocene marine vertebrate bonebed genesis in northern Chile. Palaeogeogr. Palaeoclimatol. Palaeoecol. 659, 112622.

McCartney, K., Witkowski, J., Nowakowski, R., Szaruga, A., Wróbel, R., Zgłobicka, I., 2020. Evolution of the silicoflagellate naviculopsid skeletal morphology in the Cenozoic. Mar. Micropaleontol. 156, 101820.

McCormack, J., Grif, M.L., Kim, S.L., Shimada, K., Karnes, M., Maisch, H., Pederzani, S., Bourgon, N., Jaouen, K., Becker, M.A., Jöns, N., Sismaventura, G., Straube, N., Pollerspöck, J., Hublin, J., 2022. Trophic position of *Otodus megalodon* and great white sharks through time revealed by zinc isotopes. Nat. Commun. 13, 2980. https://doi.org/10.1038/s41467-022-30528-9.

Miller, K.G., Wright, J.D., Browning, J.V., 2005. Visions of ice sheets in a greenhouse world. Mar. Geol. 217, 215–231.

Montemagni, C., Villa, I.M., 2025. Dating deformation along shear zones by the 40Ar/39Ar method: a review. Italian Journal of Geosciences 144, 250–263.

Muizon, C., de DeVries, T.J., 1985. Geology and paleontology of late Cenozoic marine deposits in the Sacaco area (Peru). Geol. Rundsch. 74 (3), 547–563.

Nelson, J.S., Grande, T.C., Wilson, M.V.H., 2016. Fishes of the world. Fishes of the World, fifth ed. https://doi.org/10.1002/9781119174844

Nobile, F., Lambert, O., Bianucci, G., Amson, E., Bosselaers, M., Bosio, G., Pellegrino, L., Malinverno, E., Di Celma, C., Urbina, M., Collareta, A., 2025. Surviving a Dark Age: The Oldest Baleen-Bearing Whales (Cetacea: Chaeomysticeti) of Pacific South America (Lower Miocene, Peru). Life 15, 452. https://doi.org/10.3390/life15030452.

Nyberg, K.G., Ciampaglio, C.N., Wray, G.A., 2006. Tracing the ancestry of the great white shark, *Carcharodon carcharias*, using morphometric analyses of fossil teeth. J. Vertebr. Paleontol. 26, 806–814.

Perez, V.J., 2022. The chondrichthyan fossil record of the Florida Platform (Eocene–Pleistocene). Paleobiology 48, 622–654.

Perez, V.J., Godfrey, S.J., Kent, B.W., Weems, R.E., Nance, J.R., 2019. The transition between Carcharocles chubutensis and Carcharocles megalodon (Otodontidae, Chondrichthyes): lateral cusplet loss through time. J. Vertebr. Paleontol. 38, e1546732.

Perez, V.J., Pimiento, C., Hendy, A., González-barba, G., Hubbell, G., Macfadden, B.J., 2017. Late Miocene chondrichthyans from Lago Bayano, Panama: functional diversity, environment and biogeography. Journal of Paleontogy 91, 512–547. https://doi.org/10.1017/jpa.2017.5.

Pilger, R.H., 1981. Plate reconstructions, aseismic ridges, and low-angle subduction beneath the Andes. Geological Society of America Bulletin 92, 448–456.

Pimiento, C., González-Barba, G., Ehret, D.J., Hendy, A.J.W., MacFadden, B.J., Jaramillo, C., 2013. Sharks and rays (Chondrichthyes, Elasmobranchii) from the late Miocene Gatun Formation of Panama. J. Paleontol. 87, 755–774. https://doi.org/10.1666/12-117.

Pufahl, P.K., Grimm, K.A., 2003. Coated phosphate grains: proxy for physical, chemical, and ecological changes in seawater. Geology 31, 801–804. https://doi.org/10.1130/G19658.1.

Purdy, R.W., Schneider, V.P., Applegate, S.P., Mclellan, J.H., Meyer, R.L., Slaughter, B.H., 2001. The Neogene sharks, rays, and bony fishes from Lee Creek mine, Aurora, North Carolina. In: Ray, C.E., Bohaska, D.J. (Eds.), English. Smithsonian Institution Press, Washington D.C., pp. 71–202

Reichmann, K.A.R., Mahoney, M.G., Long, D.J., Shimada, K., 2025. Dental variations in the crocodile shark, *Pseudocarcharias kamoharai* (Lamniformes: Pseudocarchariidae): implications for fossil *Pseudocarcharias*. Journal of the Ocean Science Foundation 45, 36–47. https://doi.org/10.5281/zenodo.18049120.

Reinecke, T., Louwye, S., Havekost, U., Moths, H., 2011. The elasmobranch fauna ofthe late Burdigalian, Miocene, at Werder-Uesen, Lower Saxony, Germany, and its relationships with Early Miocene faunas in the North Atlantic, Central Paratethys and Mediterranean. PALAEONTOS 20, 1–170.

Rivera, T.A., Storey, M., Zeeden, C., Hilgen, F.J., Kuiper, K., 2011. A refined astronomically calibrated 40Ar/39Ar age for Fish Canyon sanidine. Earth Planet Sci. Lett. 311 (3–4), 420–426.

Saillard, M., Hall, S.R., Audin, L., Farber, D.L., Regard, V., Hérail, G., 2011. Andean coastal uplift and active tectonics in southern Peru: 10Be surface exposure dating of differentially uplifted marine terrace sequences (San Juan de Marcona, 15.4°S). Geomorphology 128, 178–190. https://doi.org/10.1016/j.geomorph.2011.01.004.

Southwood, T.R.E., Henderson, P.A., 2000. Ecological Methods, third ed. Blackwell Science, Oxford.

Spell, T.L., McDougall, I., 2003. Characterization and calibration of 40Ar/39Ar dating standards. Chem. Geol. 198 (3–4), 189–211.

Sørensen, T., 1948. A method of establishing groups of equal amplitude in plant sociology based on similarity of species content and its application to analyses of the vegetation on Danish commons. K. Dan. Vidensk. Selsk. Biol. Skr. 5, 1–34.

Stucchi, M., Varas-Malca, R.M., Urbina-Schmitt, M., 2015. New Miocene sulid birds from Peru and considerations on their Neogene fossil record in the Eastern Pacific Ocean. Acta Palaeontol. Pol. 61 (2), 417–427.

Suárez, M.E., Encinas, A., Ward, D., 2006. An early Miocene elasmobranch fauna from the Navidad Formation, Central Chile, South America. Cainozoic Res. 4, 3–18.

Szabó, M., Kocsis, L., Bosnakoff, M., Krisztina, S., 2021. A diverse Miocene fish assemblage (Chondrichthyes and Osteichthyes) from the Pécs-Danitzpuszta sand pit (Mecsek Mts, Hungary). Foldtani Kozlony 151, 363–410. https://doi.org/10.23928/FOLDT.KOZL.2021.151.4.363.

Thornburg, T.M., Kulm, L.D., 1981. Sedimentary basins of the Peru continental margin: structure, stratigraphy, and Cenozoic tectonics from 6°S to 16°S latitude. In: Kulm, L.D., Dymond, J., Dasch, E.J., Hussong, D.M. (Eds.), Nazca Plate: Crustal Formation and Andean Convergence, vol. 154. Geological Society of America, Memoir, pp. 393–422.

Turner, G., 1988. Hydrothermal fluids and argon isotopes in quartz veins and cherts. Geochem. Cosmochim. Acta 52, 1443–1448.

Villa, I.M., Bosio, G., 2023. "Excess Ar" by laboratory alteration of biotite. Geology 51 (1), 121–125.

Villafaña, J.A., Campos-Medina, J., Chávez-Hoffmeister, M.F., Araya, S., Araya, B., Ledezma, L., Hernandez, Y., Ramos-Rojas, H.A., Bolomey, J., Tejo, M., Vera, F., Campoy, A.N., Arotaipe, R., Bugueño, Y., Antiquera, B., Rivadeneira, M.M., 2025. Diving into the past: a new assemblage of Neogene elasmobranch microfossils from the eastern Pacific of South America. Pap. Palaeontol. 11, e70043. https://doi.org/10.1002/spp2.70043.

Villafaña, J.A., Chávez-Hoffmeister, M.F., Cumplido, N., Campos-Medina, J., Oyanadel-Urbina, P., Rivadeneira, M.M., 2024. The fossil distribution of two pelagic lamniform sharks *Alopias vulpinus* and *Lamna nasus*, from South America. Hist. Biol. 36, 2434–2442. https://doi.org/10.1080/08912963.2023.2259409.

Villafaña, J.A., Marramà, G., Klug, S., Pollerspöck, J., Balsberger, M., Rivadeneira, M., Kriwet, J., 2020. Sharks, rays and skates (Chondrichthyes, Elasmobranchii) from the Upper Marine Molasse (middle Burdigalian, early Miocene) of the Simssee area (Bavaria, Germany), with comments on palaeogeographic and ecological patterns. Paläontol. Z. 94, 725–757. https://doi.org/10.1007/s12542-020-00518-7.

Villafaña, J.A., Nielsen, S.N., Klug, S., Kriwet, J., 2019. Early Miocene cartilaginous fishes (Chondrichthyes: Holocephali, Elasmobranchii) from Chile: diversity and paleobiogeographic implications. J. South Am. Earth Sci. 96, 102317. https://doi.org/10.1016/j.jsames.2019.102317.

Villafaña, J.A., Rivadeneira, M.M., 2014. Rise and fall in diversity of Neogene marine vertebrates on the temperate Pacific coast of South America. Paleobiology 40, 659–674.

Villafaña, J.A., Rivadeneira, M.M., 2018. The modulating role of traits on the biogeographic dynamics of chondrichthyans from the Neogene to the present. Paleobiology 44, 251–262.

Wipf, M., Zeilinger, G., Seward, D., Schlunegger, F., 2008. Focused subaerial erosion during ridge subduction: impact on the geomorphology in south-central Peru. Terra Nova 20 (1), 1–10.

Zachos, J., Pagani, M., Sloan, L., Thomas, E., Billups, K., 2001. Trends, rhythms, and aberrations in global climate 65 Ma to present. Science 292, 686–693.

Zimmermann, J.-L., 1970. Contribution à l'étude de la déshydratation et de la libération de l'argon des micas. Geochem. Cosmochim. Acta 34, 1327–1350.